An *In Situ* Laser-Induced Fluorescence System for Polycylic Aromatic Hydrocarbon-Contaminated Sediments

Prepared for:

Marc Tuchman, Project Officer
Project Number GL975149-01-0

Prepared by:

Joseph Aldstadt
Chemistry Department
University of Wisconsin – Milwaukee

Randy St. Germain
Dakota Technologies, Inc.

Timothy Grundl
Geosciences Department

Robert Schweitzer
Schweitzer Consulting

Submitted to:

United States Environmental Protection Agency
Great Lakes National Program Office
Chicago, Illinois

FINAL REPORT
May 2002

TABLE OF CONTENTS

FIGURES & TABLES

DISCLAIMER

The U.S. Environmental Protection Agency through its Great Lakes National Program Office funded the research described here under Grant GL975149 to the University of Wisconsin-Milwaukee. It has not been subjected to Agency review and therefore does not necessarily reflect the views of the Agency, and no official endorsement should be inferred.

INTRODUCTION

Statement of the Problem

In the early 1970s the poor environmental health of the Great Lakes was recognized and both the United States and Canada banded together to form the International Joint Committee (IJC) in an effort to reverse a long trend of toxic pollutant discharge to the Great Lakes. The original Great Lakes Water Quality Agreement (GLWQA) between Canada and the Unites States was signed in 1972. Almost immediately, the IJC realized the importance of sediment-bound contamination. In 1975, the "International Working Group on the Abatement and Control of Pollution from Dredging Activities" was instituted. By 1978, a "Contaminated Sediment Task Force" was established to look at the assessment and remediation of contaminated sediments. In 1987, the United States demonstrated its support of the GLQWA by establishing, under the Clean Water Act, the "Assessment and Remediation of Contaminated Sediments" (ARCS) program. The ARCS program was specifically charged with assessing the nature and extent of sediment contamination and to demonstrate the effectiveness of selected remedial options at 5 different sites [1]. The ARCS final report was issued in 1994 and immediately the IJC identified "remediation and management of sediments contaminated with persistent toxic substances" as one of its 1995-1997 program priorities [2].

This 20-year record of study has led to a consensus that contaminated sediments are a major cause of environmental problems in the Great Lakes. All of the original Areas of Concern (AOC) that were identified by the IJC as problem sites have contaminated sediment [2]. As such, contaminated sediments represent a universal obstacle to the environmental recovery of these areas. The GLWQA defines fourteen types of ecological impacts arising from contamination. Of these fourteen impacts, eleven are affected by the presence of sediment contamination. Table I lists these eleven impacts and the number of AOCs that display each type of impact.

One of the primary organic contaminants of concern in Great Lakes sediments are polycyclic aromatic hydrocarbons (PAHs). Table II lists three chemical characteristics of representative PAH compounds. For comparative purposes, the same characteristics are listed for the familiar compounds benzene and water. These characteristics define the environmental behavior of these compounds. Inspection of Table II reveals that PAH solubilities are very low and the hydrophobic sorptive capacity (K_{ow}) is correspondingly high. This, coupled with low volatilities (Henry's Law constant) and general chemical stability mean that PAHs are environmentally persistent compounds that are strongly held to solids, both suspended particles and bottom sediment. Relatively little transport via the dissolved phase is seen. Furthermore, the high partitioning to organic carbon (as reflected by high K_{ow}) is the root cause behind the high rate of bioconcentration for these compounds and the ease with which they enter the food web. This illuminates the current dilemma facing Great Lakes managers. In spite of the fact that significant decreases in the discharge of these compounds to the Great Lakes has been achieved, a large pool exists in the bottom sediments and this pool is easily re-mobilized into the base of the food web by benthic organisms. Environmental managers cannot afford to ignore the existence of contaminated sediments.

Table I. Ecological impacts potentially associated with contaminated sediment. The numbers of Areas of Concern with such impacts are also shown (modified from [2]).

ECOLOGICAL IMPACT	HOW CONTAMINATED SEDIMENT MAY AFFECT ECOLOGICAL IMPACT	NUMBER OF AREAS OF CONCERN WITH THE ECOLOGICAL IMPAIRMENT (n = 42, % in parentheses)
Restrictions on fish and wildlife	Contaminant uptake via contact with sediment or through food web	36 (86%)
Degradation of fish and wildlife populations	Contaminant degradation of Habitat; contaminant impact through direct sediment contact; food web uptake	30 (71%)
Fish tumors or other deformities	Contaminant transfer via contact with sediment or through food web; possible metabolism to carcinogenic or more carcinogenic compounds	20 (48%)
Bird or animal deformities or reproduction problems	Contaminant degradation of habitat; contaminant impacts through direct sediment contact; food web uptake	14 (33%)
Degradation of benthos	Contact; ingestion of toxic contaminants; nutrient enrichment leading to a shift in species composition and structure, due to oxygen depletion	35 (83%)
Restrictions on dredging activities	Restrictions on disposal in open water due to contaminants and nutrients, and their potential impacts on biota	36 (86%)
Eutrophication or undesirable algae	Nutrient recycling from temporary sediment sink	21 (50%)
Degradation of aesthetics	Re-suspension of solids and increased turbidity; odors associated with anoxia	25 (60%)
Added costs to agriculture or industry	Re-suspended solids; presence of toxic substances and nutrients	7 (17%)
Degradation of phytoplankton or zooplankton populations	Toxic contaminant release; Re-suspension of solids and adsorbed contaminants, and subsequent ingestion	10 (24%)
Loss of fish and wildlife habitat	Toxicity to critical life history stages; degradation of spawning and nursery grounds due to siltation	34 (81%)

Table II. Environmentally pertinent characteristics of several PAHs [3].

	Solubility (ng/g)	Henry's Law Coefficient (atm-m^3/mol)	Octanol-Water Partition Coeffficeint (log K_{ow})
Water	—	6.6×10^{-7}	—
Benzene	$1.75 \times 10^{+6}$	5.4×10^{-3}	2.12
Benzo(*a*)anthracene	12	2.3×10^{-6}	5.90
Benzo(*a*)pyrene	3.9	2.4×10^{-6}	6.00
Benzo(*b*)fluoranthene	14	1.2×10^{-5}	6.57
Benzo(*k*)fluoranthene	0.6	1.0×10^{-3}	6.85
Pyrene	135	1.1×10^{-5}	5.09

Ecosystem health is not the only problem associated with the presence of sediment contamination. Large scale economic costs to the commercial and sport fishing industries arise from fish consumption advisories, the viability of commercial ports are threatened by restriction on navigational dredging, and municipalities have to employ more expensive water treatment techniques. Over half of the eight million cubic meters of Great Lakes navigational dredging performed between 1985 and 1989 had to be placed in some form of containment facility due to high contaminant levels. Placement of dredge spoils in a containment facility increases dredging costs three to five times [2].

Relatively slow progress has been made in the remediation of the AOCs (by 1996, only one of 43 had been "de-listed") [2]. A more recent report indicates that within the Great Lakes watershed as a whole, 33 sites are listed as past or current remediation projects and an additional 15 more are listed as upcoming sites [4]. Many of these sites are on inland waterways and as a result are relatively small. Even with these generally smaller and more accessible sites, the average cost of remediation is close to $100 per cubic meter of contaminated sediment [4].

A complex set of political, socioeconomic and scientific obstacles are impeding progress in the cleanup of these sites. One recognized scientific impediment to continued progress is the inability to define the extent of the problem. One key area has been identified by the IJC that needs additional research and development is the "accurate physical identification and differentiation of sediment deposits which allow both cost-effective assessments and clean-ups" [2].

The current practice for delineating the extent of sediment contamination at any given site comes from the installation of expensive networks of discrete sampling sites. Sediment is obtained from core samples that are often times vertically blended before laboratory analysis. Blending decreases analysis costs, but results in poor vertical discretization. Original identification of the AOCs was based on sampling networks with spacings that were hundreds of meters apart. This is clearly insufficient coverage upon which to base a decision as to the most suitable remediation technique. Active remediation efforts require a more detailed understanding of site conditions and typically must install a more complete — and more expensive — sampling network with spacings on the order of tens of meters. We report on

the development of an inexpensive, rapid, vertically discrete, *in situ* technique for the measurement of sediment contamination by PAHs. The technique is an adaptation of a proven terrestrial technique; direct push testing (DPT). The technique will be invaluable in the following contexts.

- The ability to clearly assess the areal extent and concentration levels of sediment contamination. This background information is a prerequisite for any decisions on remediation designs and remediation costs.
- In-the-field guidance of dredging operations.
- Post-closure monitoring of remediated sites.
- A better understanding of bulk sedimentation rates as well as bioturbation or other re-suspension processes through vertical discretization. These processes are especially important to the understanding of contaminant flux from sediment to the overlying water column and biota.
- To serve as a practical data collection technique for the long-term analysis of trends and surveillance monitoring of sediment contamination into the future.

"Direct Push Testing": A Brief History

Direct Push Testing (DPT), also referred to as "Cone Penetrometer Testing" (CPT), is a well-established technique for geophysical and chemical characterization of subsurface terrestrial environments [5]. DPT is based on driving a conical steel tip (typically 60 apex and ~44-mm o.d. at base) under hydraulic pressure at a constant rate. The tip is advanced by sequentially attaching a series of cylindrical steel extensions or "push rods" to the assembly that are linked to one another by threadings. The thick-walled DPT push rods, typically 1 m in length, are hollow (i.e., push "rods" can be more accurately described as tubes) to accommodate sensor electronic cables, sample transfer lines, optical fiber bundles, etc. Trucks for DPT vary in size on the basis of the requirements of the site geology, from hand-operated rigs that are used to probe shallow formations of loose clay and sand to large trucks in the 20- to 40-ton range that can push to depths of 50 m or more in loose sands, although intervening layers containing coarse gravel and cobblestones will limit the maximum depths that can be reached. The load from large hydraulic rams, typically in the 20,000-kg range, is transferred to the push rods by using a hydraulic clamping system.

Direct push testing was developed as a geophysical tool early last century in the Netherlands to gather civil engineering data on the load-bearing capacity of weak soils (i.e., to identify the depth of firmer strata) [5]. In modern geophysical investigations based on DPT, changes in the force required to advance the cone through the underlying strata are recorded. For the unconsolidated and semi-consolidated geologic formations that it can successfully penetrate, DPT is advantageous compared with conventional auger well drilling in that it generates a continuous subsurface profile, causes minimal disturbance to the site, generates minimal waste at the surface, and is much faster (typically 2 cm/s).

Over the past 15 years or more, DPT has been recognized as a promising means to obtain chemical as well as geophysical information about the subsurface. DPT has been used over the last decade for a broad range of sampling and analytical techniques for the chemical characterization of the subsurface [5]. *In situ* chemical samplers can be driven into the subsurface by DPT to collect soil gas

[6,7], groundwater [8-18], or soil samples [19] at depth, thus providing a means of determining the vertical and horizontal extent of contamination. Furthermore, DPT has also been used as a means for delivering various *in situ* subsurface sensor probes, including laser-induced fluorescence (LIF) spectroscopy for semi-volatile organic compounds [20-29], x-ray fluorescence [30, 31] and laser-induced breakdown spectroscopies [32-33] for heavy metals; gamma ray spectroscopy for radionuclides [34], and various optical and electrochemical sensors, including for chlorinated aliphatic organics [35] and nitroaromatic explosives [36], respectively.

Laser-Induced Fluorescence Spectroscopy

The pioneering work in this area was done by the Naval Research, Development, Test, and Evaluation Division (NRaD) in collaboration with the Army's Waterways Experimental Station (WES) and by Dakota Technologies, Inc. (DTI). The U.S. Air Force-sponsored LIF work was carried out by Gillispie and co-workers at North Dakota State University and Dakota Technologies, Inc [37]. This work led to a commercial LIF system known as the "Rapid Optical Screening Tool" (ROST™). There are currently seven ROST LIF-DPT systems in the United States, two of which belong to the Air Force. Of the remaining five, only the one owned by Dakota Technologies is available for research and development work. The ROST system is optimized to determine two-ringed aromatics.

Fluorescence spectroscopy is one of the most widely applied spectroscopic techniques in use today. It is, by nature, a fast, sensitive and typically reversible process that makes it ideal for incorporation into a continuous screening technique that uses an optically transparent window as the conduit between the sensor and the analyte. Luminescence is the emission of light from any substance that returns to the ground state after being excited into an electronically excited state. If the bulk of the molecules emit their photons in less than a microsecond the emission is referred to as fluorescence. Emission that takes longer than this is called phosphorescence.

Fluorescence is typically observed in molecules that have an aromatic structure. One class of aromatics are the polycyclic aromatic hydrocarbons (PAHs) found in quantity in typical petroleum products. The PAHs found in sediments are also fluorescent, but they fluoresce much less efficiently than PAHs dissolved in solvent-rich environments, such as the aliphatic body that makes up the bulk of petroleum fuels. The PAHs continue to absorb the excitation light, but there is a much higher likelihood of the PAHs finding a non-radiative mechanism with which to shed the additional energy they picked up during the absorption of the excitation photon(s). In spite of this, the PAHs in sediments can still be coaxed into fluorescing well enough to allow *in situ* laser-induced fluorescence screening via a sapphire-windowed probe.

Plots of the relative distribution of the different colors (or energies) of the photons being emitted by an excited sample of PAHs are called the spectra. Figure 1 illustrates the concept of PAH absorbance and fluorescence spectra. The spectra of individual PAH species can contain enough structure (peaks and valleys) to be identified in simple mixtures in the lab. The fluorescence of PAHs in sediments however, is originating from such a wide variety and concentrations of PAHs and differing local environments (dissolved phase, sorbed to particles, microcrystals, etc.) that the resulting spectra

are broad and contain relatively little "structure" that can be used to determine which individual PAHs are responsible for the fluorescence.

Another property of fluorescence that can be measured is the varying amount of time it takes for the molecules to emit the photons after exposure to a pulsed excitation source, such as a laser. This is illustrated in Figure 2. An oscilloscope is used to observe the number of photons being emitted over time, thereby deriving additional information about the nature of the fluorophores and their environment. The different PAHs and the differing environments that exist in sediments all combine to change the observed decay times. This information is readily obtained when using a pulsed source such as the laser we used in this application. Our apparatus (described in "ROST System Description" below) allows us to investigate not only what colors are being emitted, but also how long it takes for the excited population of PAHs to emit the fluorescence photons. We use a patented method of combining the photons from four regions of the emission spectrum optically collected over 20 nm wide sections of the emission spectra at 340, 390, 440, and 490 nm.

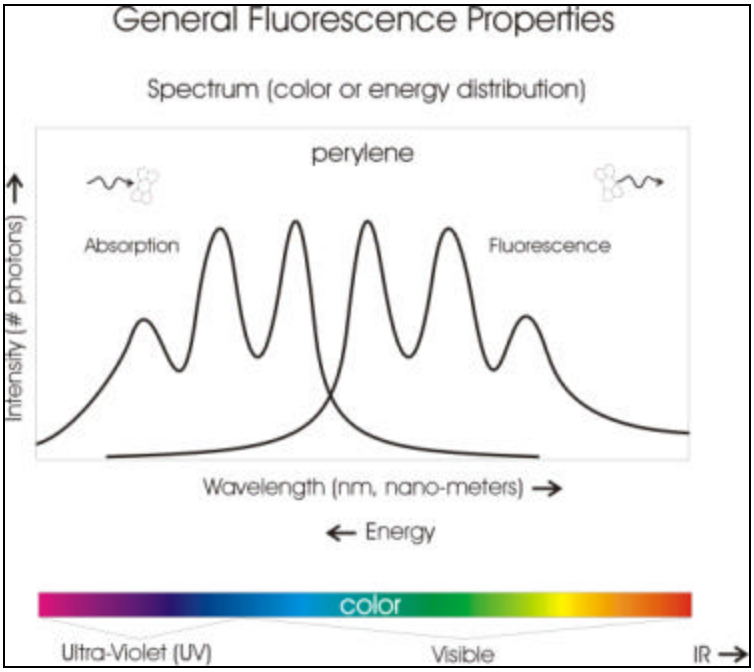

Figure 1. Spectral property of fluorescence.

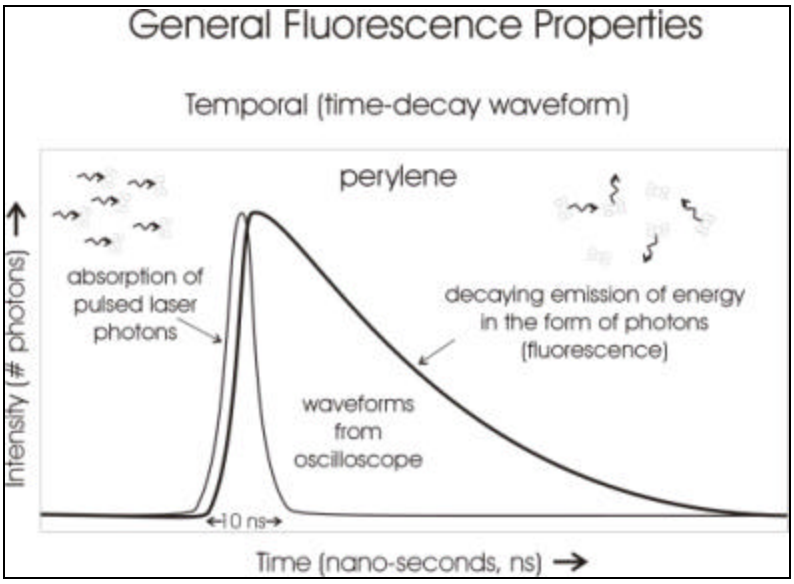

Figure 2. Temporal property of fluorescence.

These four "channels" are delayed in time through successively longer fiber optic delay lines and eventually arrive at a photomultiplier tube. The resulting waveform allows the simultaneous observation of the spectral and temporal qualities of the fluorescence. It is these multi-wavelength waveforms, measured continuously and stored vs. depth, that ultimately serve as our indicator of PAH concentration vs. depth in the sediment.

In the natural environment, additional fluorescent materials in sediments will also absorb the laser light and fluoresce intensely enough to complicate the measurement of the PAH fluorescence. Example materials include minerals such as calcite and a variety of biological materials. Both living organisms and their associated breakdown products fluoresce well enough to interfere with the observation of the fluorescence of the target PAHs. This fluorescence, along with scattered excitation laser light and Raman light generated throughout the optical train (fiber optics) will ultimately make it back to the detector, mixed in with true PAH fluorescence, and must be accounted for in some fashion. Throughout this document we will refer to all these sources of non-PAH emitted photons as "background" fluorescence, even though the true source might well be non-fluorescent (scatter) in nature.

Understanding ROST Fluorescence Waveforms

Spectroscopic techniques involve probing the target matrix with light and learning about the contents of that matrix by analyzing the light that is emitted or absorbed by the target matrix. For screening tools it is crucial to glean as much information from this light as possible in as little time as possible. The fluorescence data from ROST can be gathered quickly, but is deceptively simple. It is actually a two-dimensional data set that contains three-dimensional fluorescence information. A full

description of the multi-wavelength waveform data follows to give the reader an understanding of the data acquired during this study.

PAH Time Decay Waveforms

Each type of PAH molecule emits fluorescence over a unique time period after being excited by a pulsed excitation source such as the laser used in ROST. The emission starts out at maximum intensity, and then decays away at a rate unique to each type of PAH. The number of rings, the bonding between them, the amount of substitution on the rings, and other structural features of the molecule determine, to a great extent, the decay rate exhibited by a particular PAH. The environment in which the PAH exists also has a substantial influence on the decay rate. Quenching, which refers to any process that causes a decrease in the decay time (as well as the intensity) of the fluorescence, is dependent on a myriad of matrix dependent conditions.

Figure 3 illustrates the differing decay times one might observe for four different PAHs, along with the time profile of the laser pulse that excited them. There are large populations of PAHs being excited and while some begin emitting immediately, other individual PAH molecules "wait" many nanoseconds before emitting a photon. Figure 3 is a picture of the distribution of times that the PAHs are remaining in the excited state before emitting photons. The bold curve in Figure 3 illustrates the fluorescence decay profile that would result if all four PAHs fluoresced simultaneously and with the same intensity. This same concept applies in harbor sediments however the fluorescence decay profile observed in sediments is not made up of equal amounts of fluorescence from the various PAHs found in them. The spectra emitted by and the relative fluorescence yields of the different PAHs are all quite different, but the concept is still valid. The

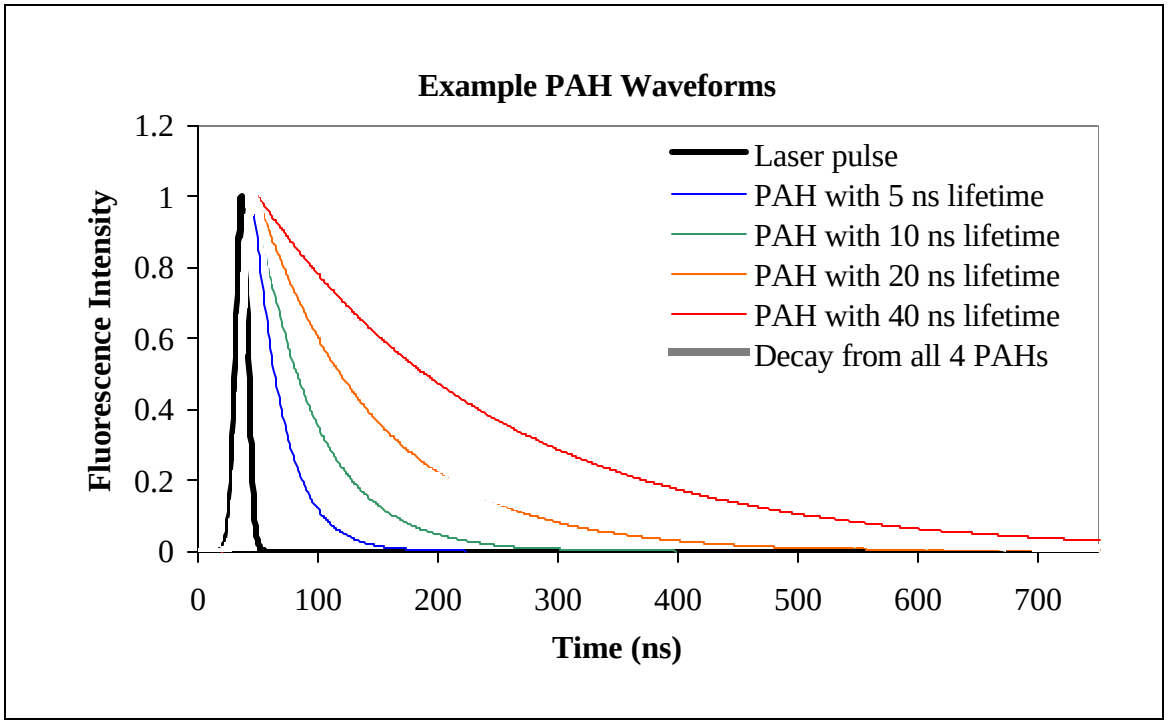

Figure 3. Examples of the temporal nature of fluorescence.

decay profile of the PAHs observed in the sediment results from the decay profiles of a mixture of different PAHs, along with fluorescence from other materials in the matrix. It should be noted that there is no predictable trend between decay rate and structure like the trend that exists between spectrum and structure as described below.

Fluorescence Spectra of PAHs

Figure 4 depicts the fluorescence emission spectra of the same four PAHs used in the temporal example in Figure 3. The fluorescence emission spectrum of a pure PAH is simply a graphical representation of the energy distribution of photons that are emitted from a large population of the PAHs as they release energy that was absorbed from the excitation laser beam. Spectra of pure PAHs such as these are typically acquired by dissolving a sample of the pure PAH in a pure solvent that does not fluoresce.

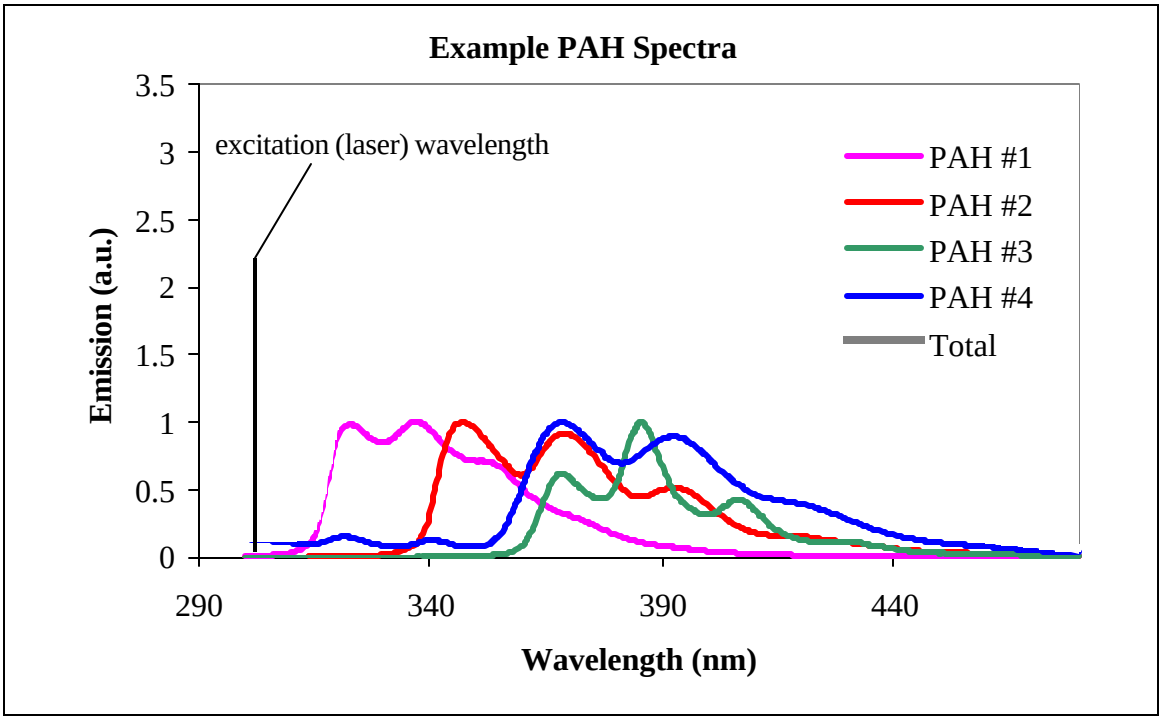

Figure 4. Examples of spectral fluorescence.

The laser wavelength is also shown in Figure 4, demonstrating the principle that fluorescence occurs at longer wavelength (lower energy) than the excitation wavelength. The basic trend is toward longer wavelength emission as more rings are added or substitution increases. Naphthalene emits at around 340 nm and the spectra "red-shift" as the number of rings increase. Another general property of fluorescence is that for a pure PAH the emission spectrum remains the same regardless of the

wavelength of the excitation light. This is not true for mixtures however, because changing the excitation wavelength might well change which PAHs are being excited and to what degree. The bold spectrum in Figure 4 is the combined spectra of all 4 PAHs. This is a simplified illustration of the total fluorescence of a mixture of different PAHs. Any change in the relative amounts of the differing PAHs or changes in the matrix in which they exist will cause a change in the spectrum of light actually emitted.

The fairly well defined structure (multiple peaks, valleys, and their various positions) of the spectra in Figure 4 suggests that perhaps algorithms could be used to directly extract information about the relative concentrations of the individual PAHs. While this is possible for very simple mixtures (two to three PAHs) under controlled conditions, the algorithms quickly fail when many PAHs are present and interference fluorescence from humics, fulvics, and minerals is introduced.

PAH Multi-Wavelength Waveform (MWW)

Real-world environmental samples typically contain multiple PAH compounds along with other fluorophores, and the PAH fluorescence spectra overlap to form broad and fairly featureless spectral and temporal emission (compared to pure PAH spectra). A complete record of the temporal decay waveforms across the entire spectrum would describe the fluorescence emission completely. Such records are called wavelength-time matrices (WTM). To create a WTM, the emission selection monochromator is scanned from wavelength to wavelength, monitoring the pulsed emission vs. time at each wavelength with an oscilloscope.

Figure 5 contains the WTMs of diesel, jet, creosote, and gasoline on sand at several thousand µg/g. The difference between the contaminants is clear and identification is straightforward. WTMs are excellent for identifying/classifying the PAH fluorescence of environmental samples because of the unique information that both dimensions of PAH fluorescence exhibit when acquired in unison. While WTMs make different contaminants readily discernable from one another, they are three-dimensional and large. Also, the screening tool must be held still while the measurement is being made. All of these qualities make WTMs unwieldy for environmental screening tools that are designed to continuously log (typically 1 Hz) the presence of PAHs vs. depth.

Because WTMs are so difficult to implement in screening mode, DTI developed a multiple-wavelength waveform (MWW) technique that allows multi-dimensional PAH fluorescence measurements to be acquired "on the fly". Figure 6 illustrates this concept. Select regions of the spectrum are monitored for their temporal response. The responses are optically delayed and recombined, and the resulting responses converge to form one two-dimensional waveform. There is sometimes overlap between the "channels" with long decay times, and the spectral regions being monitored are fewer and farther between than WTMs, but the resulting waveform still retains a unique combination of spectral and temporal fluorescence information that makes speciation and identification of PAH mixtures possible. Figure 7 illustrates the unique waveform produced by a variety of common PAH-containing environmental contaminants.

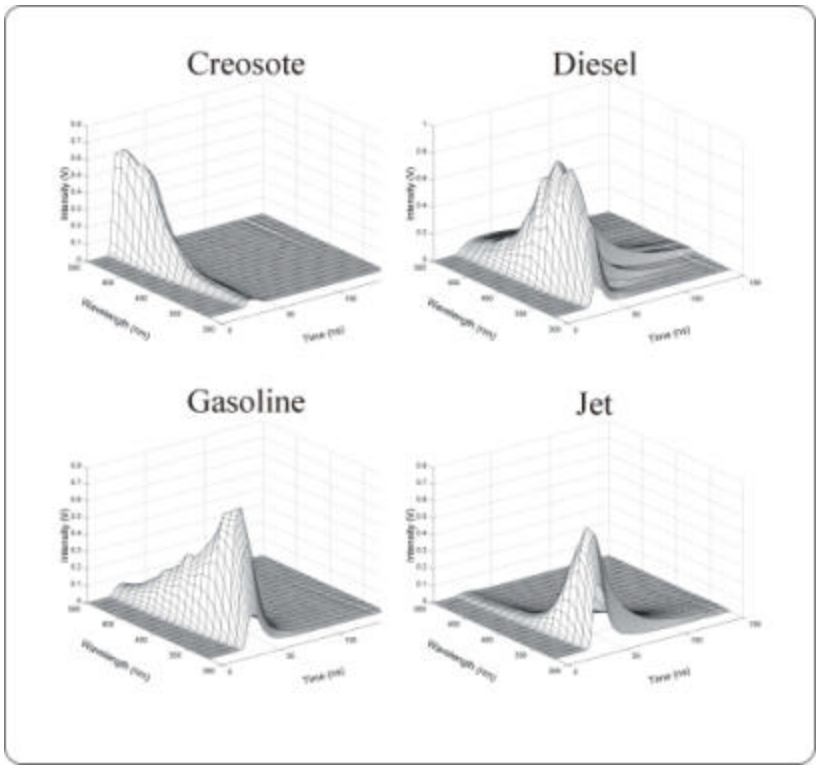

Figure 5. Example wavelength-time matrices of common contaminants on sand.

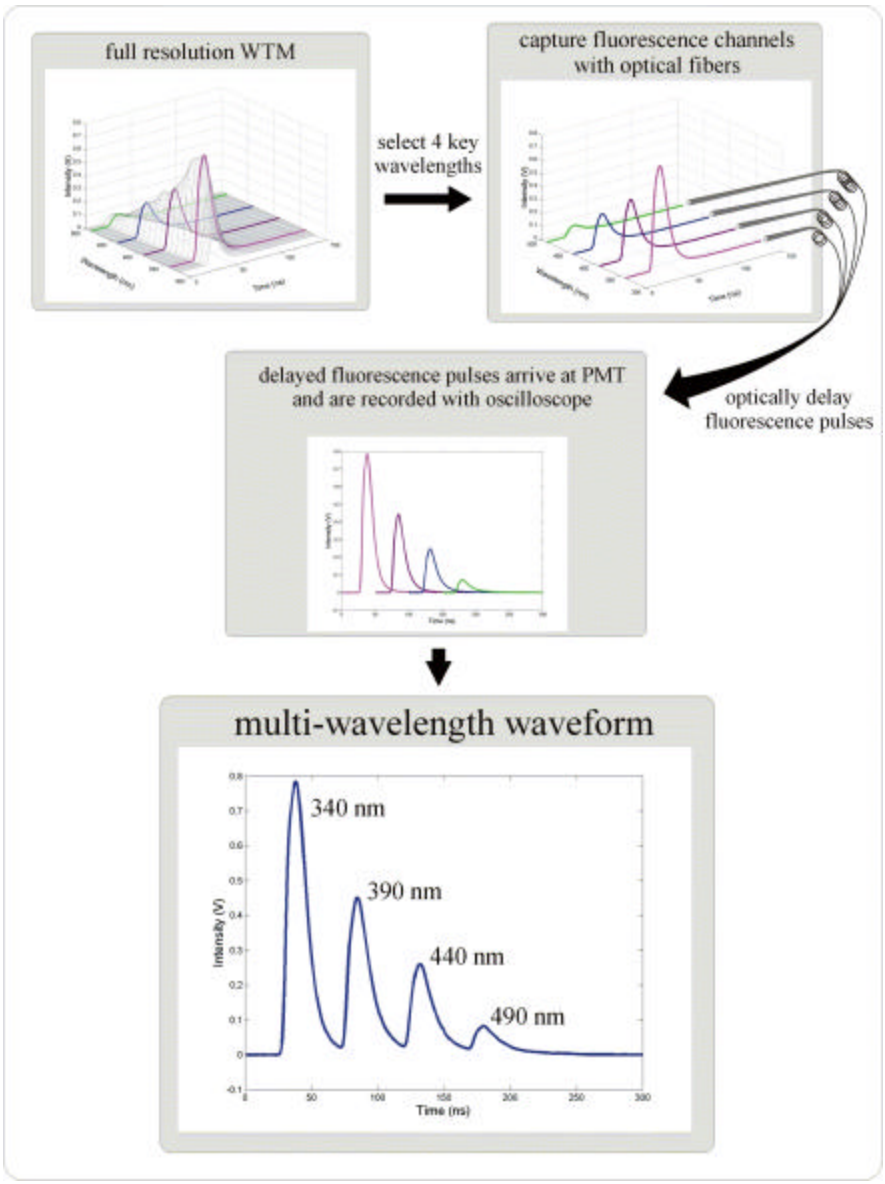

Figure 6. Multi-wavelength waveform concept.

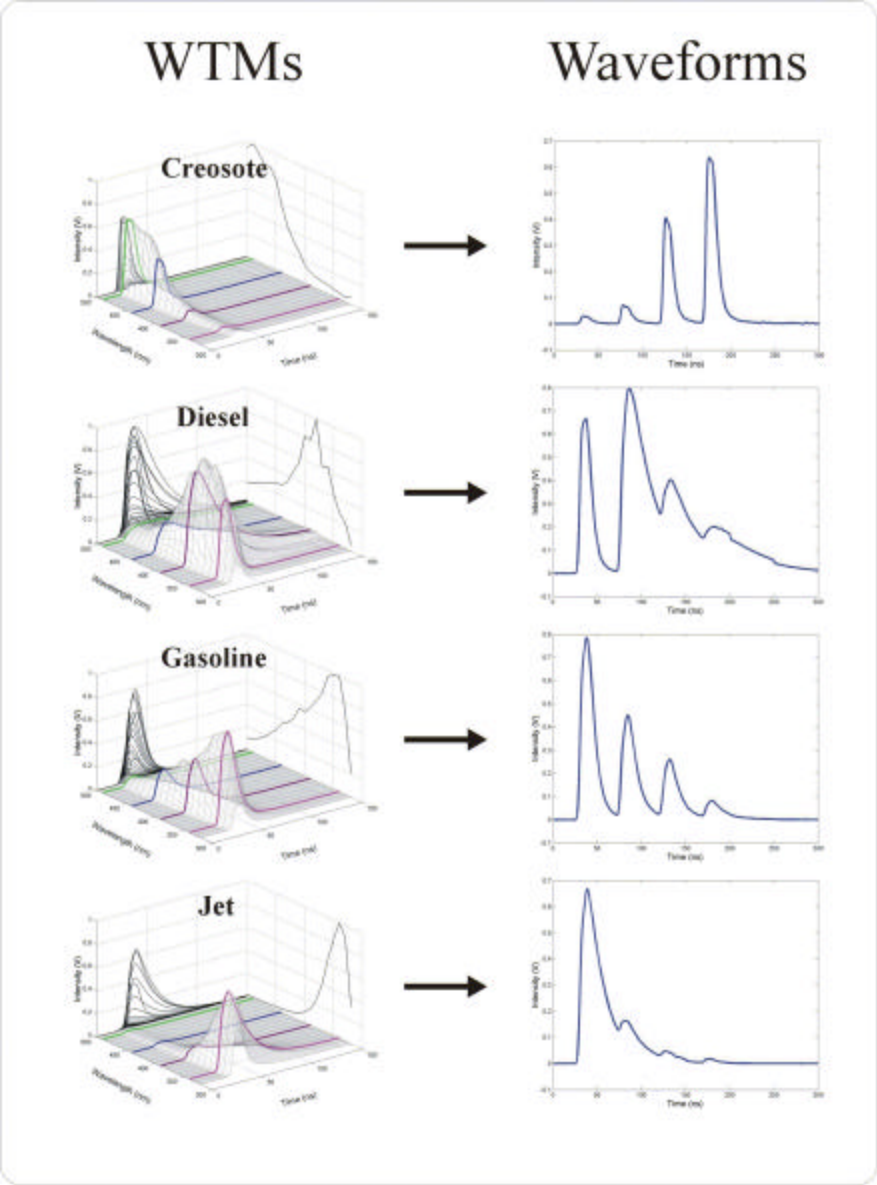

Figure 7. Waveforms of common contaminants.

FVD Colorization

The waveforms that are continuously logged vs. depth with ROST contain a wealth of information, but to make this information easily interpretable in fluorescence vs. depth (FVD) log format, the data is further reduced to a one-dimensional data set that can be plotted vs. depth. DTI developed a technique that effectively converts the shape of the waveforms into colors. These colors are then used to fill in the area under the FVD that represents the total fluorescence measured at each point in the

FVD. Figure 8, derived from data from a coal tar delineation project, illustrates the technique of colorizing the FVD according to the shape of the waveforms.

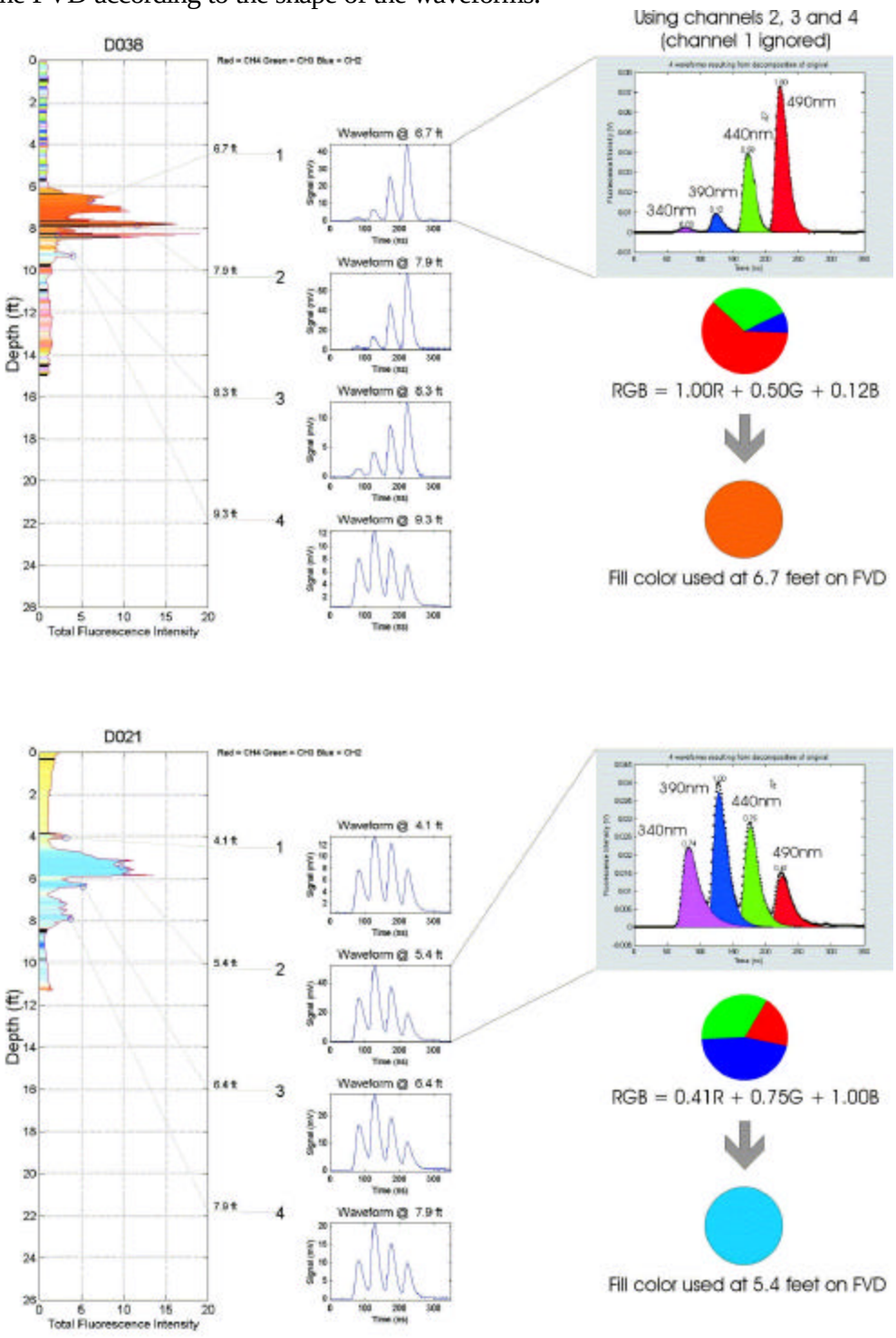

Figure 8. An illustration of how color-coding is performed.

The result is a data presentation technique that allows the user to assess similarities or changes in the waveform shapes vs. depth by simply observing the colors that represent the shape of each and every waveform in the data set. This technique was used on the sediment measurements made in this project, both in the lab and in the field. It should be noted that *black* indicates that the algorithm for generating color failed to de-convolve the waveform.

The colorization technique is limited to using three of the channels as a result of the red, green, and blue (RGB) color definition which computer colorization systems typically implement. The first three channels (340, 390, and 440 nm) were used to colorize the data in this study. The 490 nm channel was used in a quantitative sense, but was ignored for the colorization. Note that Figure 8 is an illustration from a previous study in which the 340 nm channel was ignored. It should be noted that a strictly temporal change (where only the decay times change, not the spectrum) would not necessarily result in a color change, since the ratios of the three channels used might remain constant even though the area under the waveform itself will increase or decrease.

An added benefit of this technique is that it provides insight for situations where non-linear response behavior is encountered. Many contaminants do not fluoresce with concentration in a linear fashion. For instance, a 10-fold increase in PAH concentration might produce very little or no increase in total fluorescence intensity. However, a spectral or temporal shift often does continue to occur with changes in concentration due to energy transfer, photon cycling, and other phenomenon. The color of the FVD fill continues to darken or shift in color, acting as an indicator of a change in the fluorescence of the sample, alerting the analyst to a possible increase in concentration.

PAHs in Harbor Sediments: "*Ex Situ*" LIF

In addition to the use of LIF in terrestrial sediments, LIF spectroscopy has also been successfully used in the detection of PAHs in sub-aqueous environments (i.e., laboratory analysis of the sediment by LIF). One of the key obstacles to the discrimination of contaminants in aqueous environments is the presence of high background levels of fluorescent humic substances. This problem was successfully overcome in marine sediments by using time-resolved LIF spectroscopy [38,39]. This differentiation is based on the fact that humic substances typically exhibit quite short-lived fluorescence emission (fluorescence lifetimes of 4 ns) whereas PAH fluorescence is more long-lived (fluorescence lifetimes as long as 128 ns).

PAHs in Harbor Sediments: Our Approach

In this report, we will describe the development of an adaptation of the proven terrestrial DPT-LIF technique used for the detection of PAHs for the *in situ* characterization of PAHs in freshwater sediments. This technique provides for the rapid, vertically discrete quantitation of PAH compounds with the following specific objectives:

- To adapt LIF-DPT techniques for the *in situ* detection of PAH contamination in submerged harbor sediments.
- To develop an *in situ* sediment sampling system for the collection of submerged harbor sediments that directly correspond to the LIF depth profile.
- To demonstrate the ability of this system to detect PAHs in sediment samples and its applicability as a tool to accurately delineate the extent of sediment contamination in Milwaukee Harbor.

Once the physical development of the delivery platform and sampler was in place, development shifted to the acquisition and interpretation of LIF-DPT measurements taken in the field. There are several important tasks that the data analysis focused upon. The first task was to identify the individual species contributing to the overall fluorescence signal. A second task was to remove background signals. A third task was to provide relative concentrations of the species detected and to relate these relative concentrations to true concentrations in a quantitative manner.

In Situ LIF of PAHs in Harbor Sediments: Data Interpretation

The description of LIF waveforms (see "Understanding ROST waveforms" section above) alludes to the complex interplay between the relative concentrations of individual PAHs, their fluorescence yields, spectral and temporal behavior and the presence of a variety of matrix-dependent background fluorescence signals. It is not possible to directly ascertain the contribution of a particular PAH to the total fluorescence signature by a simple summation of standard PAH spectra. However the wealth of information that is contained in each MWW matrix can be extracted by use of advanced chemometric data analysis.

Chemometric analysis was used to both define background noise and to quantify species contributing to overall fluorescence. Chemometrics is the application of mathematical and statistical methods to the collection and analysis of data. It becomes important in such areas as signal processing, design and optimization of experiments, development of calibration models, and classification of data points via clustering and pattern recognition algorithms.

The chemometric analysis for the research described in this report falls into the category of "mixture analysis". This is because the data collected in our work consist of fluorescence spectra that are a summation of the fluorescence spectra of the individual PAH components. Classical chemical analysis requires the use of a chemical separation step to provide selectivity for the individual components, but ideally chemometrics allows the separation of the component signals and background signals mathematically from the collected spectra. Most mixture analysis techniques use an approach in which a new set of variables (factors) is created, and actual chemical components in the sample are related to the factors in a way that allows the mathematical separation of the individual chemical components.

Quantitative model building was chosen as the tool to allow the identification of PAHs in sediment via LIF. Model building requires the analysis of multiple samples by both a primary method (GC-MS) and a secondary method (LIF). The primary method establishes the "true" concentrations of

the PAHs in the sediment samples, while the secondary method is the method by which one would like to perform routine measurements of PAHs. The set of data resulting from the analyses of the samples by both the primary and secondary methods is termed the calibration set. A mathematical tool is then used to establish a correlation (model) between the concentration data and the LIF spectra. This model can then be used to predict the concentrations of PAHs in sediment for samples for which only LIF spectra are available. The most familiar models are univariate models – models in which only one wavelength is used to build the relationship between a spectroscopic measurement and known concentration. The technique used in this work is a multivariate method (Partial Least-Squares Regression, PLSR) in which all spectroscopic information (all 351 points in a MWW matrix) is used simultaneously to relate to concentration. Multivariate techniques have significant advantages over univariate techniques. They provide a signal-to-noise improvement, greater robustness, greater selectivity, and the ability to monitor a new sample's fit to the calibration set. PLSR is by far the most commonly used quantitative multivariate model building technique in the chemometrics community. A text by Marten & Naes provides an excellent description of multivariate methods in general and PLSR in particular [40].

There are a few simple principles that must be adhered to ensure successful model building. The first is that a wide range of data samples must be selected for the calibration set. These samples must cover a wide range of concentrations and include samples from a wide range of different sediment matrices. It is helpful to think of each sample as a data point in an *n*-dimensional data space in which *n* is the number of spectral points in the spectra collected for each sample. The second principle is that predictions can only be made for unknowns that are well represented by the points in the calibration set. The bigger the data space that is covered by the samples in the calibration set, the greater the number and variety of unknowns whose concentration can be predicted. However, the bigger this data space, the greater the number of calibration points that are needed to cover that data space completely and evenly. The point to be made is that it is not sufficient to have a wide range of concentrations represented in the calibration set. All spectral variations that might be encountered in the field must also be represented in the calibration set. A reassuring note is that the degree to which an unknown sample is represented by calibration points in the data space can be calculated, and the results of this calculation can determine the confidence that one should place on the predicted value for that point.

EXPERIMENTAL

Reagents

All chemical reagents used were analytical reagent (AR) grade or better. Reagent water (18 MΩ-cm) was prepared using a NanoPure™ filtration system equipped with an ultraviolet lamp (Barnstead-Thermolyne, Dubuque, IA, USA). PAH standards were obtained from Supelco (Bellefonte, PA, USA). All glassware was acid-washed after use for at least 48 hours in 5% (v/v) AR-grade nitric acid to remove background contamination. PAH-containing standards were prepared on the day of use. All standards were stored at 4 C.

Instrumentation & Methods for PAH Analysis

PAH analyses were conducted according protocols based on U.S. EPA standard methods; a flow-chart of the analytical process is shown in Figure 9. Samples were collected with a VibraCore and sectioned (2-6"), dried, and stored. Pressurized Fluid Extraction (PFE) was then performed in duplicate (1:1 acetone:hexane) based on EPA Method 3545 [41] implemented using a method that we developed previously for SVOCs [42]. Our PFE method resembles commercial PFE approaches (e.g., Dionex Accelerated Solvent Extraction or ASE™), but a crucial difference is that the available extraction cell that we use is inexpensive, making it more appealing to laboratories like ours that handle relatively small numbers of samples. The stainless steel extraction cells (64-mm-long pipe (7 mm i.d. and 12 mm o.d.), threaded at both ends and fitted with end caps) were obtained from Minnesota Valve and Fitting (Eden Prairie, MN, USA). An Isotemp Model 301 laboratory oven (Fisher Scientific, Pittsburgh, PA, USA.) or a Model 47900 furnace (Thermolyne, Dubuque, IA, USA) was used to heat the extraction cells. With one end of the stainless steel cell capped, a 300-mg sample (500-mg for SRM) was placed in the cell, followed by 3 mL of hexane. To ensure a good seal on the capped cell, Teflon tape was placed on the threads on both ends of the cell (not in contact with the sample). The loaded cell was then placed in an oven for a predetermined time (usually 60 min). The extraction cell was cooled to room temperature under tap water. The cell was opened, and the contents were transferred to a glass vial. A portion of the extract was transferred to a conical vial and used for GC-MS injections without further cleanup.

PAHs were determined by Method 8270C [43] using a dedicated Gas Chromatograph with Electron Ionization Quadrupole Ion Trap Mass Spectrometry (GC-MS), performed in a Clean Room environment on a Varian Saturn 2000 system (Walnut Creek, CA, USA). The GC-MS consisted of the following components: Model 3800 capillary gas-liquid chromatograph (DB-5MS column, 30 m x 0.25 mm with 0.25 µm film, J&W Scientific, Folsom, CA, USA) with Model 1079 split/splitless injector; electron impact ionization source (70 eV); Saturn 2000 quadrupole ion trap MS (10-650 m/z range, unit resolution). The automatic gain control (AGC) of the MS system was used throughout this study; mass spectra were obtained by single ion monitoring at relevant retention times with a 0.7 s scan time. Automated library searching was performed using the National Institute of Standards and

Technology (NIST) Mass Spectral Database (version 3.0). The mobile phase was ultra-high purity helium (Praxair, Milwaukee, WI, USA) at a constant linear velocity through electronic flow control.

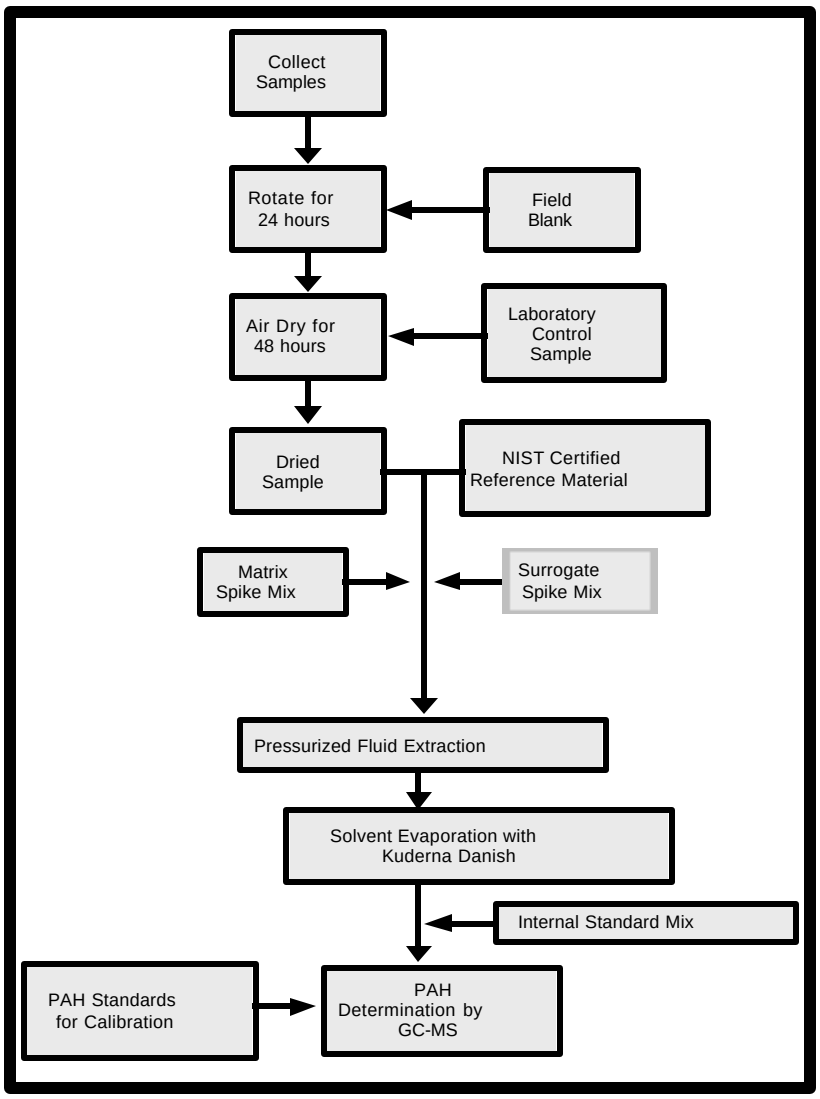

Figure 9. Laboratory analysis scheme for PAHs in sediments.

Data acquisition and reduction were accomplished using the Varian GC-MS software (vers. 5.21). GC instrument control and data acquisition were performed on a Pentium personal computer (Dell, Optiplex GX1, Dallas, TX, USA). QA/QC measures included field blanks, solvent blanks, method blanks, matrix spikes, and surrogates. Percent recovery was determined using three surrogate compounds (Nitrobenzene-d^5, Benzo(*ghi*)perylene, and 4-terphenyl-d^{14}) and matrix spikes (Naphthalene, 2-Fluorobiphenyl, Pyrene); the recoveries ranged from 80-102%.

Sixteen separate calibration models were built using Internal Standards (Naphthalene-d^8, Acenaphthene-d^{10}, Phenanthrene-d^{10}, Chrysene-d^{12}, 1,4-Dichlorobenzene-d^4, and Perylene-d^{12}); validation was performed using a contaminated river sediment (SRM 1944) obtained from the NIST (Gaithersburg, Maryland, USA); accuracy was < ±20%.

ROST System Description

The ROST system is contained in a ruggedized shipping container as shown in Figure 10. The system actually consists of a variety of sub-systems that are described in detail in this section. The numbers in each heading below refer to the equivalent numbers in Figure 10.

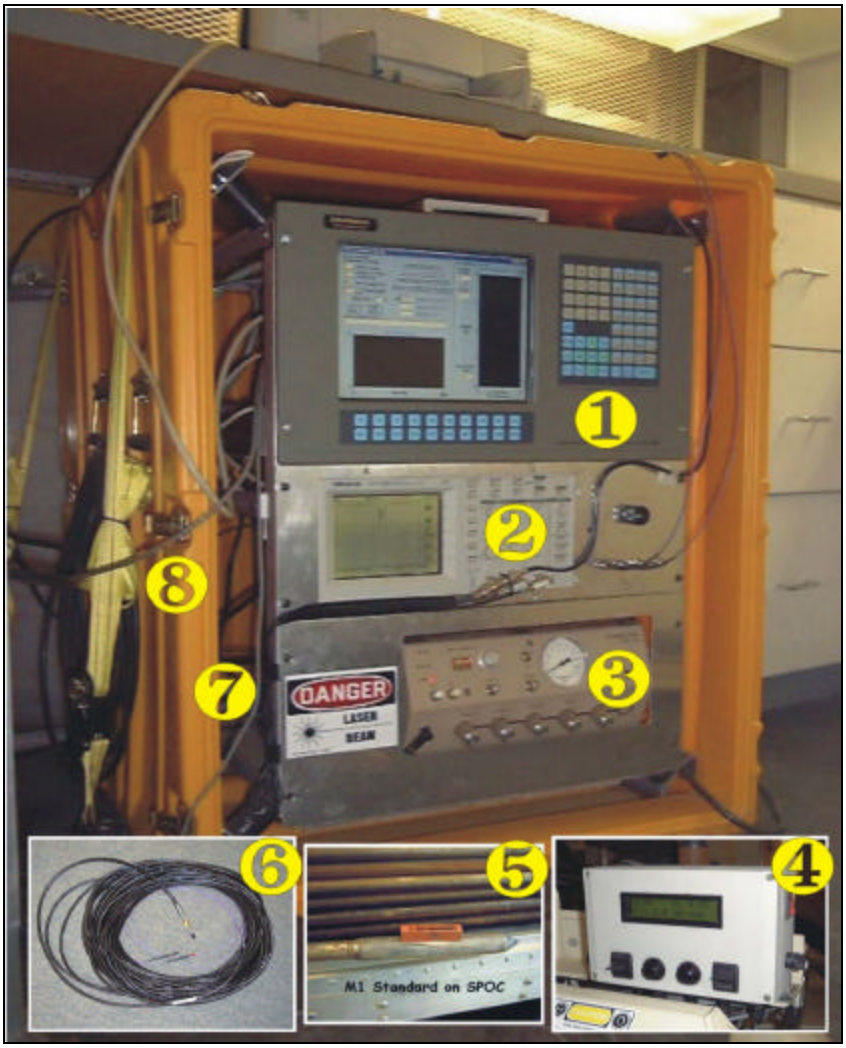

Figure 10. ROST system and key peripheral devices.

Laser (3)

The ROST system employs a pulsed XeCl Excimer laser (MPB PSX-100) that generates very fast pulses of 308 nm light (50 Hz). The width of each pulse is less than 10 billionths of a second (i.e., < 10 ns) at half height. The energy of the source radiation efficiently excites the vast majority of PAHs present within the sediments. A beamsplitter directs a fraction of the beam to an energy meter to monitor excitation pulse energy. A photodiode is positioned near the beamsplitter and serves as the trigger source for the time-resolved fluorescence measurement. A lens is used to launch the laser light into an optical fiber for delivery a sapphire window at depth.

Fiber Optic Cable (6)

The fiber optic cable consists of two 40 m silica/silica optical fibers. One fiber delivers the excitation pulse while the other is used to return a portion of the resulting fluorescence to the surface. The diameter of the optical fiber core is 365 µm. The fibers terminate in a custom-made connector at the sub-surface (see SPOC below). Because the fibers are readily broken if flexed or handled too aggressively, they are housed in a flexible polyurethane-covered stainless steel sheath with a bend radius limiting quality that effectively reduces fiber optic failure rates.

Shock-Protected Optical Compartment (SPOC) (5)

The optical fibers deliver and receive the light from a steel probe that consists of two threaded Geoprobe rods (one inch diameter) terminated with a special optics module and tip called a "SPOC". The SPOC employs proprietary elastomer supports, in combination with Swagelok™ fittings, to insure long term stability of the optical alignment along with protection against breakage. The SPOC contains a parabolic mirror that acts to turn the excitation beam 90 degrees. The beam exits the SPOC through a sapphire window that is flush-mounted on the side of the SPOC and strikes the sediment that is pressed against the window as the probe advances through the sediment. Sapphire's hardness (second only to diamond) allows it to resist scratching or breaking under all but the most severe conditions. The laser beam illuminates several mm^2 of the sediment that is exposed to the window's surface and any resulting fluorescence (along with a substantial quantity of scattered laser light) is emitted back into the window where a portion is reflected by the parabolic mirror into the return fiber for transport to the surface.

The SPOC design is watertight; a necessary attribute when probing in saturated sediments. Any leakage can result in evaporation of the intruding water into the air space within the SPOC. The resulting water vapor can cause fogging on the interior surface of the sapphire window or corrosion of the optics and hardware within the SPOC. An extra measure of humidity prevention is achieved by purging the SPOC with an inert gas immediately prior to reassembly any time it is open to the atmosphere for maintenance or adjustment.

Emission Detection System (hidden from view) (7 and 8)

The collection fiber returns the entire spectrum of light ("white light") that is collected from the sediment. Since this is a multi-channel (multi-wavelength) detection system, we must disperse the white light. The collection fiber is butt-coupled directly into an Acton SP150 imaging monochromator that disperses the white light into a "rainbow" that can sampled at four regions (340, 390, 440, and 490 nm) for detection.

Before the light is dispersed by the monochromator, the source light from the Excimer laser (308 nm) must be removed and the amount of fluorescence light must be controlled. The detector does not differentiate between laser light and fluorescence, so this laser light must be filtered out. To achieve this, a long-pass cutoff filter (320 nm CFLP) is placed immediately inside the monochromator, rejecting the vast majority of laser light, but passing the lower energy (longer wavelength) fluorescence. Butt-coupling of the fiber to the monochromator eliminates the slits that are usually found on the entrance of a monochromator. These slits are designed to control bandpass and the amount of light that enters the monochromator to avoid saturating the detector. The ROST system employs a neutral density filter wheel for controlling light levels instead. By selecting an appropriate optical density filter the light levels can be controlled with precision. The reference emitter signal (M1 described later) was attenuated in these studies while the PAH fluorescence was passed through without filtering due to its relatively low intensity.

At this point, if all four fiber optics were of the same length and were directed into the detector (PMT), all four channels would be combined into a single decay curve (waveform). To achieve separation of the four wavelengths, the photons must be time-delayed so that they strike the detector at different times. To achieve this the fiber optics are made in 10 m increments - 2, 12, 22, and 32 m in length for the 340, 390, 440, and 490 nm wavelengths, respectively. Because of the finite speed of light in the optical fiber core, these “delay lines” allow for the temporal resolution of each channel by approximately 50 ns. These four fibers are then terminated in a single large-core SMA fitting which couples to a large diameter (1500 micron) fiber optic that is 0.33 m in length. This large diameter fiber is taken through a relatively sharp bend that serves to "mix" the four fiber optic beams into one homogeneous beam. The large fiber is attached to a mount that directs the light at the photocathode of the PMT detector.

Oscilloscope (2)

The entire waveform arrives in less than 250 ns; therefore a very fast device is required to accurately record the data. The ROST system employs a 100 MHz Tektronix® TDS 220 digital storage oscilloscope capable of 1 billion samples per second (1 Gs) to record the waveforms. A 50-ohm terminator at the input of the fluorescence channel converts the current to a voltage, allowing measurement of a voltage vs. time waveform that represents the arrival of the photons at the PMT. A second channel of the oscilloscope is used to monitor an energy meter (a much slower measurement) before each test, to log the laser energy performance for maintenance/service tracking purposes. The fluorescence waveforms are displayed on the oscilloscope in real time and are retrieved from the oscilloscope via a general-purpose interface bus (GPIB) for storage and analysis. Approximately 50 laser shots are averaged for each sampling point along the test, which ends up being equivalent to a 1 Hz waveform storage rate. At the probe advancement speed used in this study, the vertical data density averaged 0.3 to 0.5 inches (0.8 to 1.0 cm).

Instrument Control & Data Acquisition Computer (1)

A rack-mounted industrial computer is used to control the ROST system and log the data to the hard drive. The computer controls the monochromator, the oscilloscope, a differential GPS beacon, and the depth control and acquisition module (DCAM). The host computer program was written in Visual Basic 5. The software provides a real time display of the test results while the test is in progress and generates a full color picture of the log at the end of the test. The waveforms are continuously

logged to the hard drive while a total FVD log is created by integrating the entire fluorescence waveform and plotting its intensity vs. depth. The final data analysis and display was done on a separate workstation.

Depth Control and Acquisition Module (DCAM) (4)

To accurately log PAH fluorescence vs. depth, it was crucial to accurately and dependably monitor the position of the probe as it was being advanced or retrieved from the sediment. Since the probe was positively engaged to a gearbox via a chain drive mechanism (direct drive), a depth sensing system was designed based on monitoring the rotation of the gearbox. A waterproof proximity sensor was mounted in a position that allowed the proximity sensor to sense the passing of the gear teeth as the gear rotated. The proximity switch is phase sensitive, allowing determination of both the speed and direction of the gearbox and ultimately the probe speed and direction.

A custom DCAM was built for this project. The DCAM controller for this project was custom programmed to correctly sense the proximity sensor and calibrated to convert the proximity sensor counts to distance (measured in feet). The DCAM's sole function is to monitor the proximity sensor, calculate the speed, direction, and distance traveled, display the result on a digital display, and make the results available to the ROST computer via RS-232 protocol.

Calibration and Normalization

The ROST system response depends on a host of factors. These include laser energy, fiber termination quality, neutral density filter selection, parabolic mirror efficiency, fiber length, and others. To account for changes over time and location, a single point calibration and system check is performed. A reference emitter (coined M1) is placed on the sapphire window and the response is measured. The M1 solution is permanently stored in a quartz cuvette for convenience and the measurement takes place through the wall of the cuvette. This proprietary mix of hydrocarbons fluoresces efficiently across the entire system and serves as both an indicator of system function and as a data normalization benchmark.

The total fluorescence intensity (area under the waveform) of M1 serves to normalize the data from the push that immediately follows the reference emitter measurement. All the FVD logs are presented as a percentage of the signal achieved with M1. The area under every waveform in the data set is integrated, resulting in a picovolt-seconds unit (pVs). These values are divided by the pVs measured for M1, and the result is multiplied by 100. The result is a log with x-axis units of percent of M1. This creates a normalized data set that takes into account the entire system performance, from laser to oscilloscope. The shape of the M1 waveform acts to guide the operator in assessing proper alignment of the detection system. The relative contribution for each channel and the shape of M1 waveform is monitored for consistency to insure that the waveforms remain consistent from day to day.

Field Sampling Methodology

A key part of this project was to develop a means to deliver the LIF probe into submerged harbor sediments and to develop a means to collect sediment samples at depth from within the DPT rod co-linear with the optical window. These samples were needed to directly calibrate LIF response to measured PAH concentrations in the same sediment. Both the delivery vehicle and sediment sampler were designed to operate from a surface vessel in depths as great as 45 feet.

Shipboard Delivery Vehicle

The shipboard delivery vehicle (SDV) consists of a steel framework supporting a 9-foot tall DPT-like pushrod assembly. This framework has a rectangular base consisting of a 3.5 x 5 foot steel plate with a hole in the center through which the DPT rod is advanced. Total dry weight of the SDV is 780 pounds. The pushrod assembly is advanced via a sliding trolley attached to a chain drive. Motive force is provided by a 1/3 horsepower, variable speed, reversible electric motor and gear reduction drive. Maximum insertion speed is 2 cm/sec.

The SDV is fitted with flotation tanks that can be evacuated and filled with air via electrically driven solenoid cut-off valves. By emptying or filling the tanks with air, the SDV can be automatically set for positive buoyancy (floating), nearly neutral buoyancy (a submerged weight of ~50 pounds) or fully weighted (flotation tanks full of water). Requisite air control valving, interior water level sensors, and electrical harness are all housed on the SDV.

Ancillary equipment housed on the SDV includes automatic limit switches to avoid over advancement of the pushrod assembly, video camera and lights, level indicators, an "on-bottom" indicator switch and a gauge to measure depth of pushrod penetration. The penetration gauge is capable of continuously monitoring at mm resolution, in both up and down directions, the location of the LIF probe beneath the sediment-water interface.

The SDV is completely submersible and when in use is attached to the surface vessel only by a lifting cable at the top and an umbilical cord. The umbilical contains a Kevlar strength member, a multi-conductor electrical cable for power (120 VAC and 240 VAC) as well as valve control and switch cabling, a fiber optic cable (with two optical lines), a video feed cable and compressed air. All controls are lead to a weatherproof control box on the surface vessel. The physical detachment from the surface vessel allows field work to be performed in other than flat calm conditions as would be necessary if the probe was being advanced directly from the surface vessel. The maximum depth of operation is limited only by the length of the umbilical.

The SDV was specifically adapted for use with the research vessel maintained by the EPA Great Lakes National Program Office (GLNPO) (the *R/V* Mudpuppy) although it will work with any vessel that has AC power and a large enough lifting capacity to handle the SDV. For use with the *R/V* Mudpuppy, the floating SDV was cinched to the square bow of the vessel, and pushed to the site of interest. After the vessel was anchored on-site, the SDV was released and the flotation tanks partially filled with water to the preset negative buoyancy of 50 pounds. The SDV was gently lowered to the bottom by the lifting cable, the flotation tanks completely filled with water and the pushrod assembly advanced into the sediment. As the LIF probe, located near the tip of the pushrod assembly, advanced

into the sediment a real-time fluorescence signal was collected and a paper copy was immediately printed. Upon completion of the push, the sequence was reversed: the pushrod was retracted, the SDV re-floated, cinched to the vessel and moved to the next site. The entire sequence, including anchoring and transit time, took approximately 30 minutes. Figure 11 shows the SDV with the components labeled. Figure 12 shows the SDV in transit attached to the *R/V* Mudpuppy.

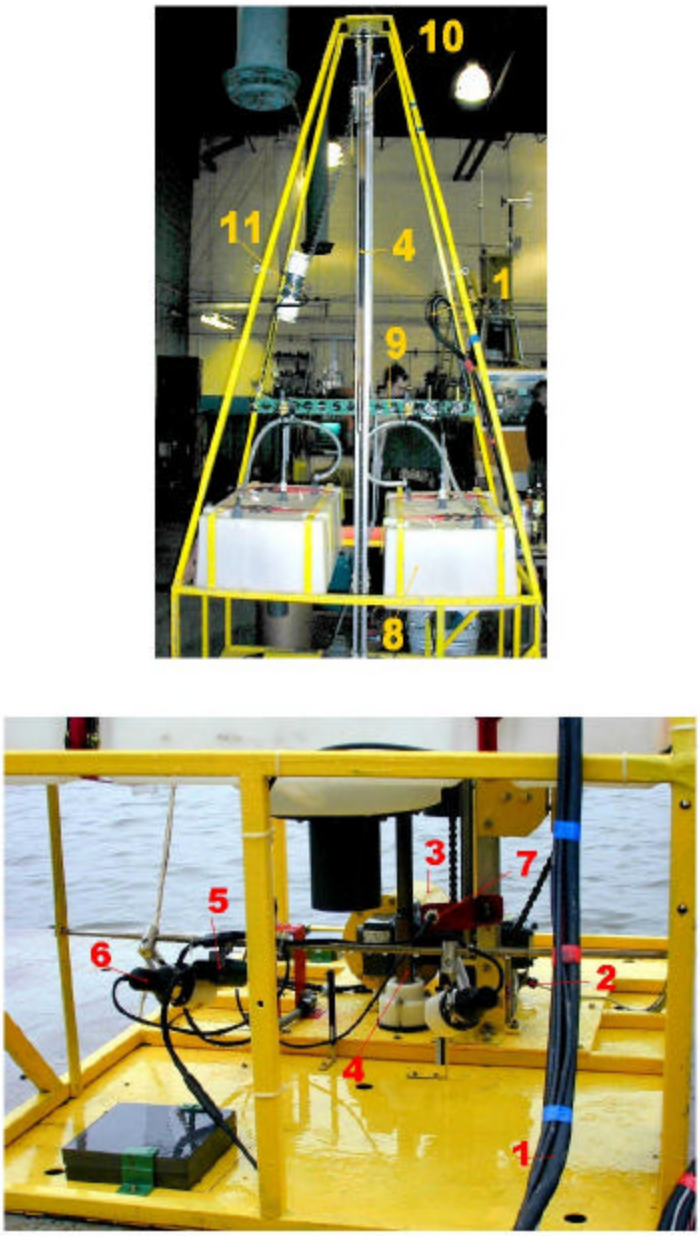

Figure 11. SDV components and key peripheral devices.
Umbilical (1), DCAM sensor (2), drive motor (3), push rod (4), video camera (5), video light (6), "over-penetration" limit switch (7), flotation tanks (8), air valving manifold (9), push rod drive head (10), sediment sampler valving manifold (11).

Figure 12. The R/V Mudpuppy in Milwaukee Harbor.
The SDV is cinched to the bow of the vessel.

In Situ Sediment Samplers

Two sediment sampler designs were studied. Both samplers operate from within the pushrod assembly above the LIF probe. Both collect sediment from a position approximately six inches above and directly in line with the LIF window. The pushrod assembly can be stopped at any point, either during insertion or retraction, to take a sample.

The first design was based on retracting a sleeve in the pushrod thereby exposing a spring-loaded door that opened into the sediment. Closing the sleeve back down over the door pushed the door shut and served to collect sediment. Retracting and closing the sleeve was accomplished by reversing the direction of the entire pushrod assembly. The sleeve was held closed during normal pushrod insertion/retraction by an electrically actuated, pneumatic latch. The latch was actuated from the main control box on the surface vessel. This design never became fully operational and was not used during field-testing.

The second sampler was in essence a small horizontally-oriented core barrel that extended and retracted laterally out of the pushrod assembly. The core barrel was 1 cm in diameter by 3 cm in length and could collect ~ 1 g of dry sediment. This amount was sufficient for GC-MS analysis preceded by pressurized fluid extraction (as described in the Experimental section). The core barrel extruded through a perforated septum that was designed to seal the end of the core barrel before and after sample collection. The core extruded over a sliding base plate that provided sufficient suction (like a syringe) to keep the sediment in the core barrel as it retracted into the pushrod assembly. An electrically actuated, 2-way pneumatic cylinder provided the motive force for core barrel extension.

Retraction was accomplished by a coil spring inside the pushrod assembly. The core barrel was actuated from the main control box on the surface vessel. The requisite pneumatic valve manifold was mounted in a watertight compartment housed on the SDV. Operation in the field consisted of removing the pushrod assembly from the re-floated SDV (via the removal of one drift pin), removing the septa and transferring the sediment into a sample container with a spatula. The core barrel was then cleaned, a new septum was installed, and the pushrod assembly returned to the SDV.

This design did reach the field-operational stage and was used to collect several confirmatory samples during field-testing. The sampler was damaged midway during field-testing and design refinements are envisioned.

Field Testing Program

Development of the SDV and integration with the LIF spectroscopic system included significant field-testing from a crane at the dock of the Great Lakes WATER Institute, the WATER Institute vessel (*R/V* Neeskay) and the EPA vessel (*R/V* Mudpuppy). A similar testing program was employed for the sediment samplers. Only a description of the final field demonstration (on the *R/V* Mudpuppy) is included in this report.

The final field demonstration concentrated on the lowermost reaches of the Kinnickinnic River in Milwaukee, WI. During the course of 2.5 days, ten sampling stations were occupied along the Kinnickinnic River, from the mouth (near the Jones Island sewage treatment plant) upstream to a point halfway between the 1st Avenue and Becher Street bridges. Figure 13 is an annotated aerial photograph showing the sampling locations and pertinent landmarks. Table III lists the station numbers, latitude-longitude locations and other pertinent data for each location.

At least one LIF push was performed at each site. At station 6.5, a replicate push was done after re-positioning the SDV about one foot away from the original location. This was done to check on the reproducibility of the LIF signal. At station 5.5 a replicate push was performed at a faster penetration rate. This was done to examine how much of the vertical resolution was lost by a faster insertion speed. The sediment sampler was used to collect samples at stations 1, 3, 5, and 7. On a subsequent push the probe hit refusal and the SDV tipped over with the pushrod assembly extended in the sediment. This damaged the sampler and no more samples were collected in this manner.

Immediately following completion of the LIF fieldwork, 8 stations were re-occupied and VibraCore samples collected. The original LIF sites were re-located for coring by use of the shipboard GPS system. The accuracy of this system is such that re-location was within 15 feet. Core samples were collected in 3-inch clear plastic tubes. Core tubes were immediately sealed in the field and were stored frozen in the dark to await sectioning and GC-MS analysis. A total of 44 individual sediment samples were analyzed by GC-MS, of which 36 came from these core samples. The remaining eight were collected from the sediment surface via Ponar ("clam-shell") sampler in other parts of Milwaukee Harbor. Aliquots of all 44 samples collected for GC-MS analysis were directly exposed, in the laboratory, to the LIF window and a LIF spectrum obtained. These samples were used as the calibration set to build the chemometric model that related LIF spectra to the known concentration of

each PAH compound. Note that in this calibration set GC-MS and LIF measurement pairs were performed on exactly the same sediment thereby eliminating any bias from differences in sample location or stratigraphy.

Table III. Descriptions of the stations occupied during field testing.

Station	Latitude	Longitude	Water Depth	LIF Push Depth	VibraCore Depth	Description
Number	(north)	(west)	(feet)	(feet)	(feet)	
1	43° 01.3674'	87° 54.2120'	29.0	9.37	2.58	near Jones Island treatment plant
2	43° 01.1133'	87° 54.2216'	15.5	9.60	2.17	at asphalt plant loading dock
2.5	43° 00.8970'	87° 54.2414'	24*	9.54	--	at the coal loading dock
3	43° 00.7100'	87° 54.3387'	14.0	9.56	--	at wall just downstream of coke plant inlet
4	43° 00.6957'	87° 54.3491'	16.2	9.54	9.00	right in the middle of the coke plant inlet
5	43° 00.5195'	87° 54.4458'	21.3	9.60	3.00	75 meters east of KK Ave. bridge
5.5	43° 00.4940'	87° 54.6223'	5.6	9.54	5.42	just off the fishing boat dock
5.5 push 2	43° 00.4940'	87° 54.6223'	5.6	9.55	--	penetration rate is 2.5 times faster
6	43° 00.4972'	87° 54.7009'	5.6	9.54	2.58	just upstream from 1st Street bridge
6 push 2	43° 00.4972'	87° 54.7009'	5.6	4.85	--	hit refusal and tipped sled over
6.5	43° 00.4957'	87° 54.7765'	7.9	9.57	8.17	halfway from station 6 to bend in river
6.5 push 2	43° 00.4957'	87° 54.7765'	7.9	9.55	--	replicate push
7	43° 00.4713'	87° 53.8263'	8.0	9.54	9.33	on the corner where river turns to the south
* depth varied from 23 to 25 feet across the bottom of the SDV						

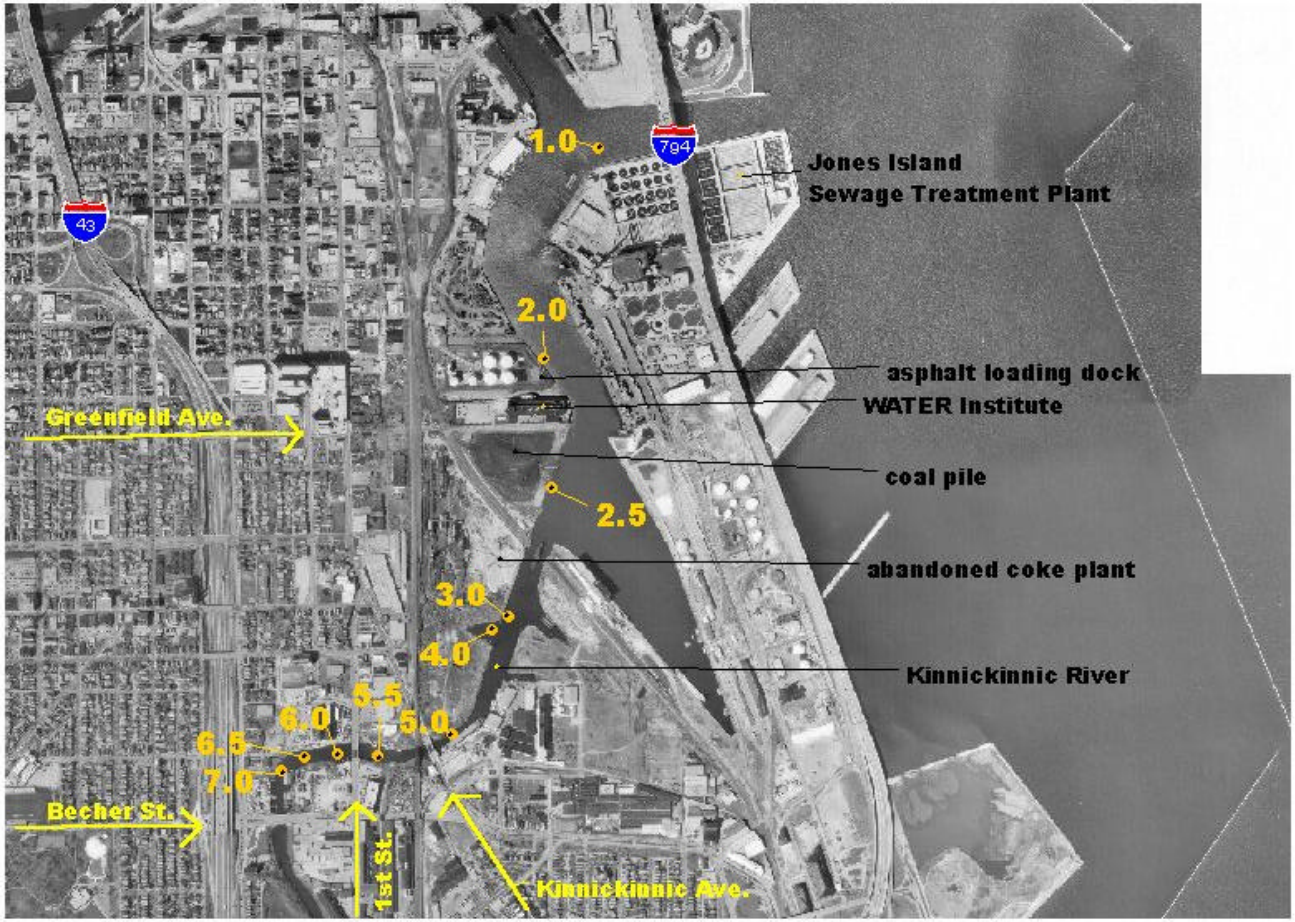

Figure 13. Aerial photograph of study area.
LIF test stations denoted by station number. North is to the top of the photograph.

Data Analysis

The calibration set was used to build a PLSR model relating the LIF spectra to PAH concentration for each of the 16 PAHs. The LIF spectra were collected by smearing a sediment sample that had been collected by the VibraCore on the optical window of the LIF probe. These spectra were then related to a GC-MS analysis (using EPA 8270C protocol) of the same sediment. These data are referred to as "uphole" data. "Downhole" data refers to spectra collected from in-the-field LIF pushes. Twenty replicate spectra were collected and an average spectrum was generated after removing the first and last two spectra in a set of twenty. This was repeated for each sample in the calibration set. Some preliminary PLSR models were built to test three common preprocessing strategies. For this data it was found that auto-scaling gave the best results. For each of the 351 points in the MWW matrix, the mean and norm was calculated over each sample. Each sample was then subtracted by the mean and divided by the norm. This operation gives each of the 351 data points an equal weighting. The PLSR algorithm can still give more weight to spectral points that provide important correlations with concentration as opposed to those that contain little useful information. While applying the models to the downhole data, it was found that one further preprocessing step was needed. The LIF intensities of the downhole data are significantly different from the intensities of the uphole data. Thus, it was necessary to scale each MWW between 0 and 1 for both the calibration set and the downhole data before the auto-scaling over variables was performed. Even though absolute intensity information is lost, PLSR still successfully built quantitative models by looking at the relative intensities of the 351 spectral points for each MWW.

PLSR includes a data dimensionality reduction aspect analogous to principal components analysis. Associated with this is the question of the number of latent variables to use for a given model. As the number of latent variables is increased, the percentage of variance explained by the model for both the concentration and spectral domains generally increase to a maximum of 100%. In addition, the ability of the model to predict the concentrations of the data samples in the calibration set also increases. This predictive ability is generally quantified by a root mean square error of calibration calculation (RMSEC) where:

$$RMSEC = \sqrt{\frac{\sum (actual_i - predicted_i)^2}{n}}$$

where n = total number of samples.

After a certain number of latent variables, however, the ability of the model to predict the concentration of PAHs for spectra not in the calibration set begins to decrease. The use of a prediction set, in which the samples are not used for calibration, allows the generation of a root mean square error of prediction (RMSEP) that can be used to find an appropriate number of latent variables. For sets of data with small numbers of samples it is possible to use another measure of merit called the root mean square error of cross validation (RMSECV). With this method, a separate model is built for each sample in the calibration set. Each model is built using all samples in the calibration set except for the sample whose value is being predicted. The result is a predicted value for each sample where the predicted value for a given sample is achieved with a model in which that sample is not used in the building of the model. The RMSECV serves the same purpose as the RMSEP, but allows the model development to proceed

without needing to split the available set of data into a calibration and prediction set. RMSECV analysis was used for the research described in this report. After determining the appropriate number of latent variables for each PAH model, the full data set was used to rebuild the model with all samples used in the calibration set. The resulting model was used to predict downhole PAH values.

It is important to be able to catch the cases in which a spectrum will not result in a valid prediction. In the current work, a very simple test has been implemented. The cosine of the angle between the unknown MWW and the closest MWW in the calibration set is calculated for each unknown MWW. By normalizing all vectors before doing the vector comparison, the maximum value will be 1.0 (for a perfect match). If the cosine of the angle value is low, however, the ability of the model to make an accurate prediction for that unknown cannot be guaranteed. An added benefit of this outlier check is that sediment samples for outliers could be taken and the resulting data points (after LIF and GC-MS analysis) could be added to the model, thereby increasing the predictive ability of the model. It is also important to establish concentration limits below which the models cannot give reasonable predictions (a *defacto* limit of detection based on the models). The calculation of an average relative error for the entire sample set versus subsets in which the predicted PAH concentration is above some threshold limit is one attempt to achieve such a *defacto* limit of detection.

RESULTS & DISCUSSION

Field Performance of the SDV/LIF System

The field-testing program successfully demonstrated the ability of the SDV and the associated LIF system to rapidly collect fluorescence–depth profiles in the field. Within a 2.5 day time frame, 10 profiles were collected, 2 of which were replicated. A full 9-foot penetration was achieved at all 10 profile sites. In only one case did the LIF probe hit refusal (at a depth of 5 feet) and that was in an attempt to replicate a third site (station 6). The ability to penetrate these sediments is considerably better than the equivalent ability of the VibraCore system. This is evident by inspection of Table III that shows only two VibraCores penetrating to a depth of 9 feet.

Printed results were obtained within minutes of completing a LIF push. An example of total fluorescence–depth profiles obtained in the field is shown in Figure 14. These plots contain not only total intensity, but also spectral information. The spectral information is shown at four specific wavelengths in the waveform plots as well as by the color-coding of the main profile. The color-coding scheme is explained in the "FVD colorization" section.

Figure 14 shows the two replicate pushes performed at station 6.5 and serves to illustrate the reproducibility of the LIF signal. These two pushes were performed within 1 foot of each other and show essentially identical spectral information (color changes) and very similar total fluorescence response. Figure 15 shows the loss in vertical resolution when the penetration rate is increased from 1.0 to 2.5 cm/sec. It was concluded that the minimal time savings realized by a faster penetration rate was not worth the loss in vertical resolution. The standard penetration rate for all stations was kept at 1 cm/sec. Appendix A contains all of the total fluorescence–depth profiles collected during the course of this demonstration.

PAH Quantification by Chemometric Data Analysis

Total fluorescence in any given sediment reflects not only the presence of PAH compounds, but also any other fluorophore that may be present in the sediment. To extract PAH fluorescence from background fluorescence, a chemometric model based on PLSR analysis was performed as described in the "Data analysis" section. Initial PLSR analysis was performed on a set of 44 individual sediment samples for which PAH concentration and the corresponding LIF response was known. The initial PLSR analysis identified one anomalous sample (station 6.5, depth 4.58-4.75 feet) that could not be modeled. The exact cause of this anomalous behavior is unknown, but could be from an unidentified pollutant, or an unusual background fluorescence signal. This sample was excluded from further analysis and the final chemometric model was built using the remaining 43 individual samples. The resulting chemometric model discriminated fluorescence from each individual PAH compound and allowed the prediction of individual PAH concentrations from total LIF signal.

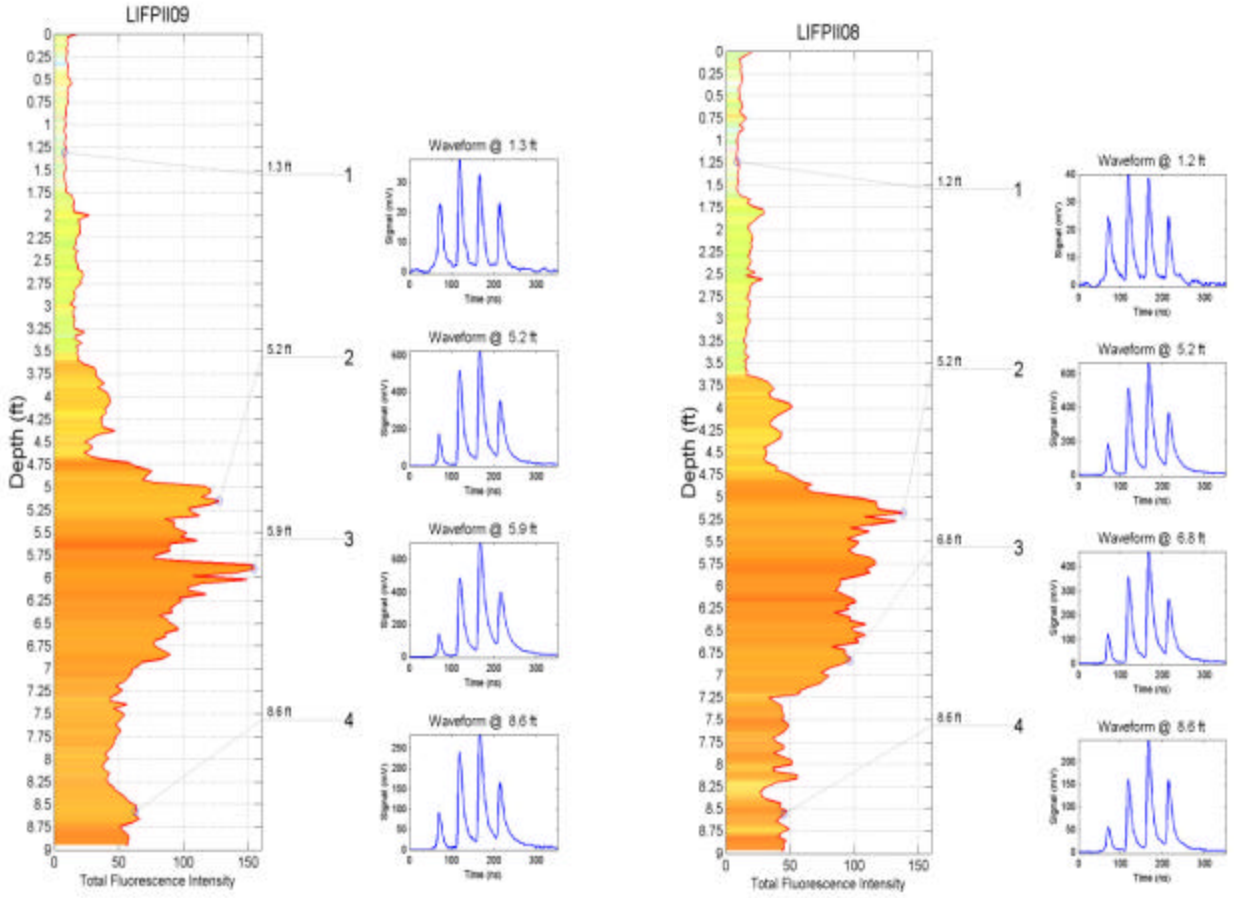

Figure 14. Depth profiles of total fluorescence.
Two replicate pushes taken at station 6.5 are shown. Replicate pushes were made within one foot of each other. Spectral plots to the right of the profiles indicate the relative intensity of fluorescence signal at 340, 390, 400 and 490 nm.

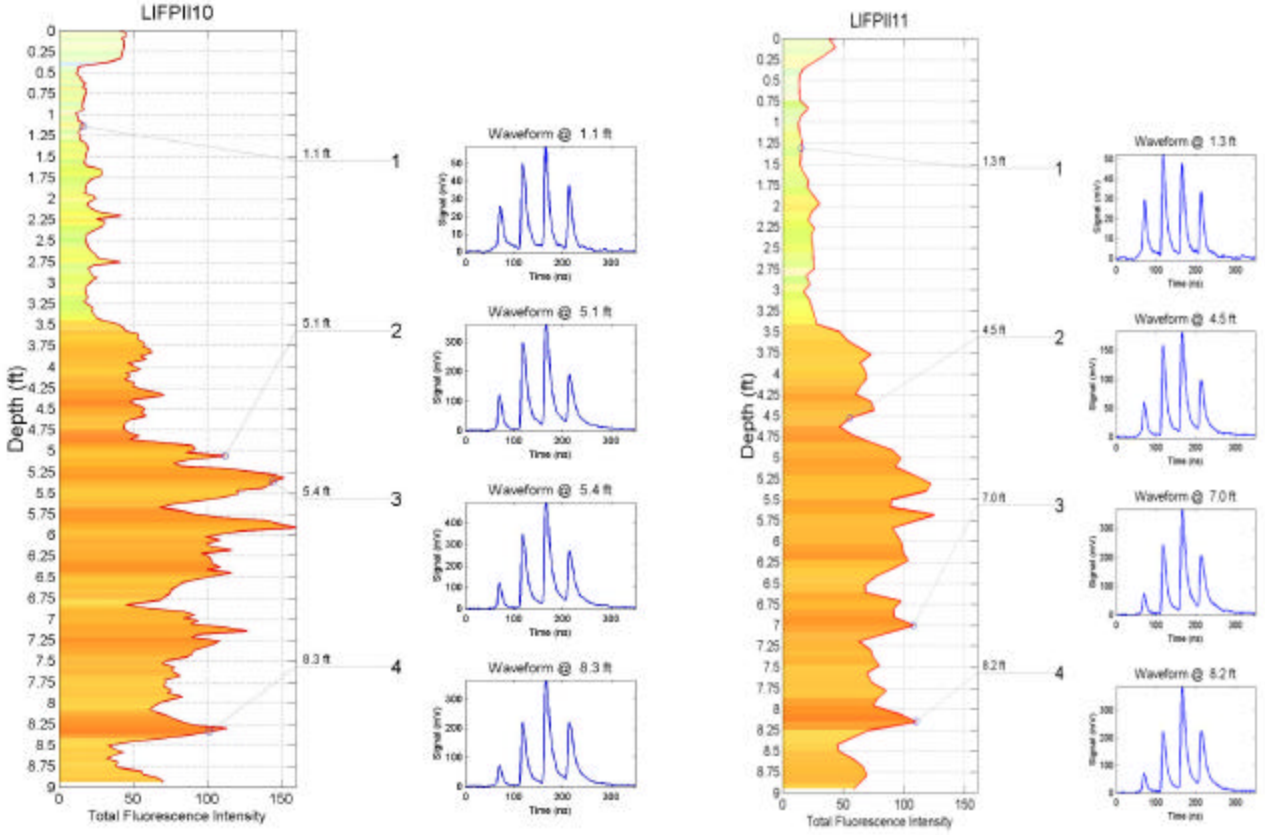

Figure 15. Depth profiles of total fluorescence for two replicate pushes taken at station 5.5. Replicate pushes were taken within one foot of each other. Profile on the right was taken at a penetration rate 2.5 times faster than the profile on the left. Spectral plots to the right of both profiles indicate the relative intensity of fluorescence signal at 340, 390, 400 and 490 nm.

Total PAH concentration in the calibration set ranged from 10 to 650 µg/g dry weight. Basic sediment characteristics of a subset of these 43 samples were measured. The subset was chosen to span the widest range in characteristics observed in the field. Results are shown in Table IV. A wide range in grain size distribution (% sand, silt, clay and carbonate) is evident. As would be expected in harbor sediments, percent organic carbon is relatively high (1.2 to 5.4 %). Our ability to quantify PAH levels and to discriminate between background and PAH fluorescence is applicable to sediments that fall within the limits seen in Table IV.

Table IV. Gross sediment characteristics.
Data shown is for a subset of the 43 samples used in the calibration set. Samples were chosen to span the widest range in sediment characteristics observed in the field.

Station number	Depth (feet)	% Sand	% Silt	% Clay	% Carbonate	% Organic Carbon
1	1.75-2.25	26.0	65.0	9.0	39.3	3.7
2	0.75-1.25	48.0	42.4	9.6	46.2	3.4
4	2.75-3.25	22.1	65.3	12.7	38.8	2.6
4	6.75-7.25	42.9	39.3	17.8	68.3	3.4
5.5	1.92-2.08	35.2	57.8	7.0	39.3	2.2
5.5	4.92-5.08	22.1	66.3	11.7	39.7	3.3
6	1.75-2.25	69.9	24.2	6.0	32.5	3.4
6.5	1.50-1.67	92.5	5.0	2.5	34.6	1.2
6.5	2.50-2.67	42.0	51.0	7.0	38.9	4.1
6.5	3.00-3.17	31.9	60.0	8.1	37.4	5.4
6.5	3.58-3.75	27.8	62.2	10.0	39.1	4.1
6.5	4.58-4.75	17.9	62.7	19.5	39.4	2.0
6.5	8.08-8.25	16.0	68.7	15.3	38.4	3.7
maximum		92.5	68.7	19.5	68.3	5.4
minimum		16.0	5.0	2.5	32.5	1.2

Figure 16 shows the match between measured and predicted concentrations for representative 2, 3, 4, and 5-ring PAH compounds. GC-MS concentrations for all 43 samples are given in Appendix B. Structural formulas for all 16 PAHs are also provided in Appendix B. Plots of the match between measured and predicted concentrations, along with the associated data tables, are given in Appendix C for all 16 PAH compounds. The match between predicted and measured concentrations, as seen in Figure 16 (and Appendix C), is sufficiently close for the technique to be used as a screening tool for all compounds except acenapthylene, dibenz(ah)anthracene and naphthalene. The measured concentrations of these three compounds in our calibration set were too low (<3 µg/g in most of the 43 samples) to allow the building of a robust chemometric model.

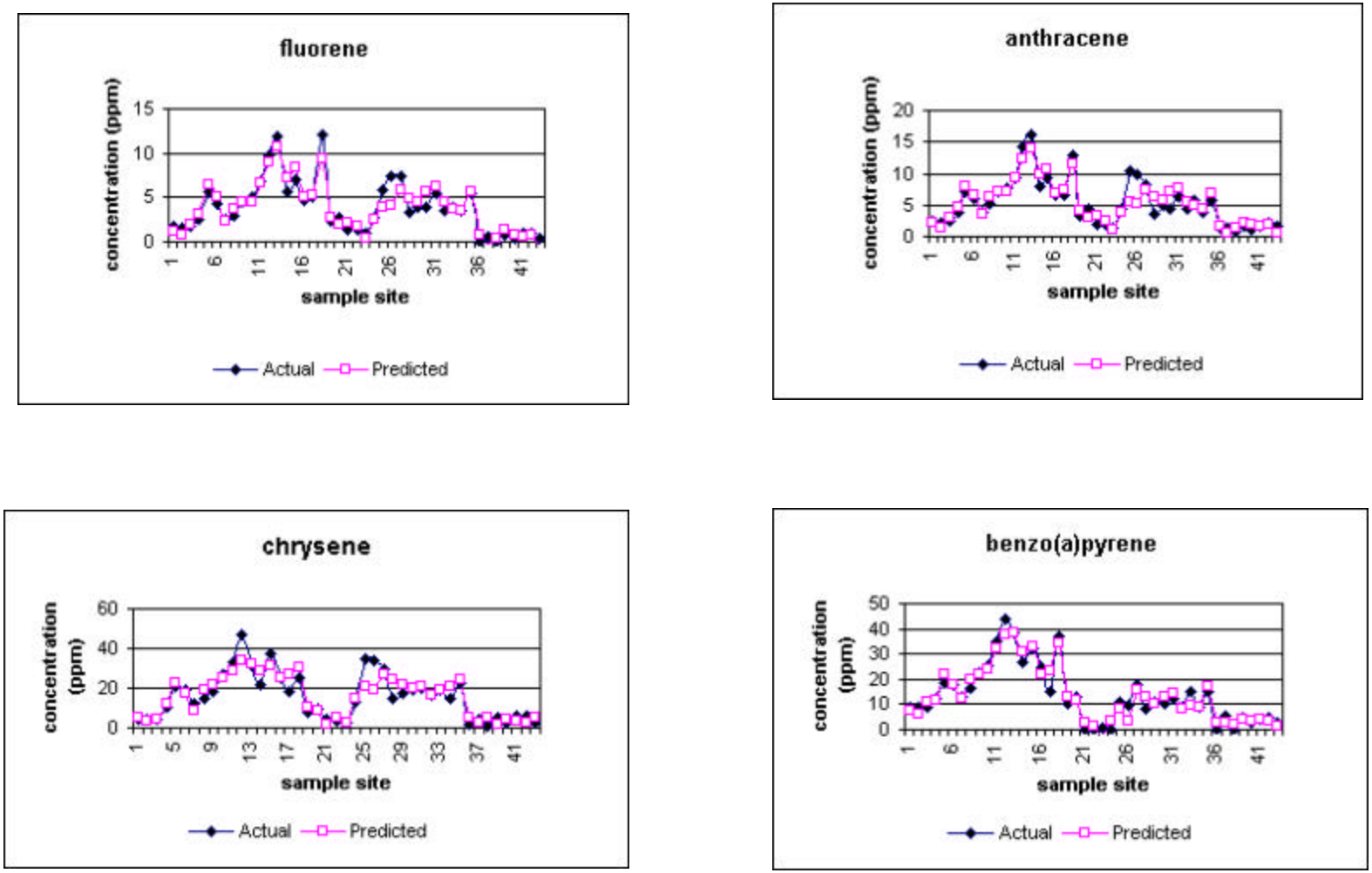

Figure 16. Predicted vs. measured concentrations of representative 2-ring PAHS.
These are: 2-ring (fluorene), 3-ring (anthracene), 4-ring (chrysene) and 5-ring (benzo(a)pyrene) PAHs. Individual samples come from station 1 (sample 1,2); station 2 (sample 3); station 4 (samples 4, 5, 6); station 5 (sample 7); station 5.5 (samples 8-18); station 6 (samples 19, 20); station 6.5 (samples 21-35); various surface samples collected in clean portions of the harbor (samples 36-43).

Several techniques were used to quantify the extent to which the chemometric model can be used as a predictive tool. The harshest measure of predictive ability is the root mean square error of cross validation (RMSECV). In essence, RMSECV analysis uses all but one of the data points to predict the concentration of the remaining point. This process is repeated until all 43 data points have been predicted from models in which each data point was *not* included. Table V lists, for each PAH, the relative errors between predicted and measured concentrations for the 43 samples in the calibrations set using RMSECV analysis. Also included is the maximum and minimum concentration observed in the calibration set. This maximum and minimum are the effective concentration range over which the predictive model is valid. Complete data tables for the RMSECV analysis are given in Appendix D.

Table V. Relative errors between measured and predicted concentrations. Error is shown for each compound as determined by root mean squared error of cross validation. Compounds in italics contain measured concentrations that were too low to make a robust prediction. RE=average relative error; TL=threshold limit in µg/g; [m]=measured concentration (minimum, maximum) in µg/g.

Compound	RE overall (%)	RE above TL (%)	TL	[m] min	[m] max
Naphthalene	312.9	114.5	1	0.0	12.5
Acenapthylene	28.9	12.8	1	0.0	2.7
Acenapthalene	71.7	24.9	2	0.0	10.0
Fluorene	45.6	27.2	2	0.0	12.1
Phenanthrene	141.0	35.7	10	0.0	95.8
Anthracene	41.8	28.7	2	0.7	16.1
Fluoranthene	123.3	41.9	10	1.2	155.4
Pyrene	86.7	42.4	10	0.0	131.2
Benz(a)anthracene	32.2	22.7	10	0.0	42.3
Chrysene	59.3	24.9	10	1.0	47.2
Benzo(k)fluoranthene	36.9	29.1	10	0.0	83.4
Benzo(b)fluoranthene	30.7	20.7	10	0.0	34.0
benzo(a)pyrene	53.0	19.3	10	0.0	44.2
Indeno(123-cd)pyrene	90.1	33.6	10	0.0	48.6
dibenz(ah)anthracene	100.9	100.9	2	0.0	11.9
Benzo(ghi)perylene	42.1	21.9	10	0.0	30.9
overall average	81.1	37.4			
average without low concentration samples	65.7	28.5			

For the chemometric model to discriminate background fluorescence from PAH fluorescence, a certain level of PAH signal is required. The three compounds that were not found in sufficient quantity (acenapthylene, dibenz(*ah*)anthracene and naphthalene) were eliminated from further analysis because

the PAH signals were too low to model. For the remaining 13 compounds, the average relative error is 65.7%. As the concentration of a particular PAH diminishes, its signal becomes difficult to distinguish from background. There exists a threshold concentration below which relative errors become increasingly large. This threshold limit has been set at 10 µg/g except for compounds in which 10 µg/g is at or near the maximum level measured. In these cases, the threshold limit was set to 1 or 2 µg/g. Using the threshold limit approach, the average relative error diminishes significantly — from 65.7% to 28.5%. Although similar in concept to a "detection limit", the threshold limit is *not* a detection limit. Detection limits have a well-defined meaning based on replicate analyses of a sample and the random nature of indeterminate errors. The threshold limit is qualitatively defined as the level below which the match between measured and modeled concentrations begins to diverge.

The chemometric models developed from this calibration set were applied to the LIF pushrod data collected at all 10 field stations, including replicate pushes. Figures 17, 18, and 19 show the depth profiles for stations 7 (farthest upstream site), 1 and 2 (farthest downstream sites), respectively. Depth profiles of all the stations are given in Appendix E. Figures 17 through 19 show both the measured total fluorescence intensity profile and a profile of the modeled concentrations of total PAHs. The former is generated directly in the field, the latter is a summation the modeled concentrations for each of the 16 individual PAHs taken at each depth. The total PAH concentration line is the 5-point moving average of modeled concentrations taken at approximately 1-cm intervals. Because LIF spectral data yields a measurement of each individual PAH, depth profiles for individual PAHs can also be generated. Example profiles of individual 2, 3, 4, and 5-ring PAH compounds are shown in Figure 20 for station 7. Complete concentration-depth data tables (available in digital format) are a part of Appendix E.

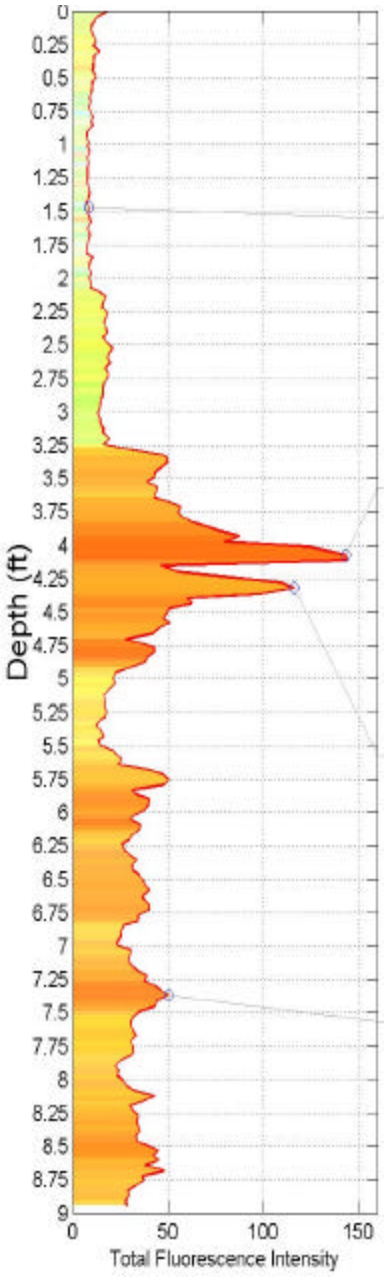

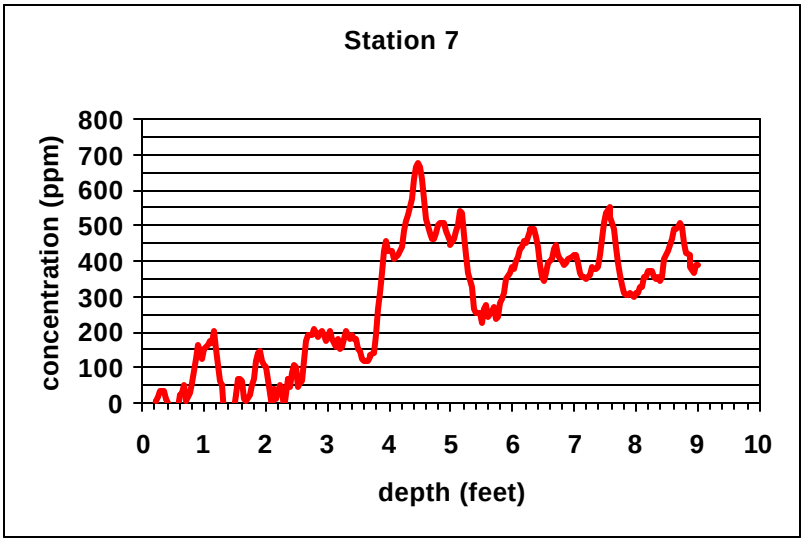

Figure 17. Plots of field fluorescence measurement and chemometric prediction: Station 7. The total fluorescence intensity profile as obtained in the field for station 7 is shown on the left. On the right is the concentration profile of total PAHs obtained after application of chemometric analysis. The concentration profile is a 5-point moving average of individual measurements.

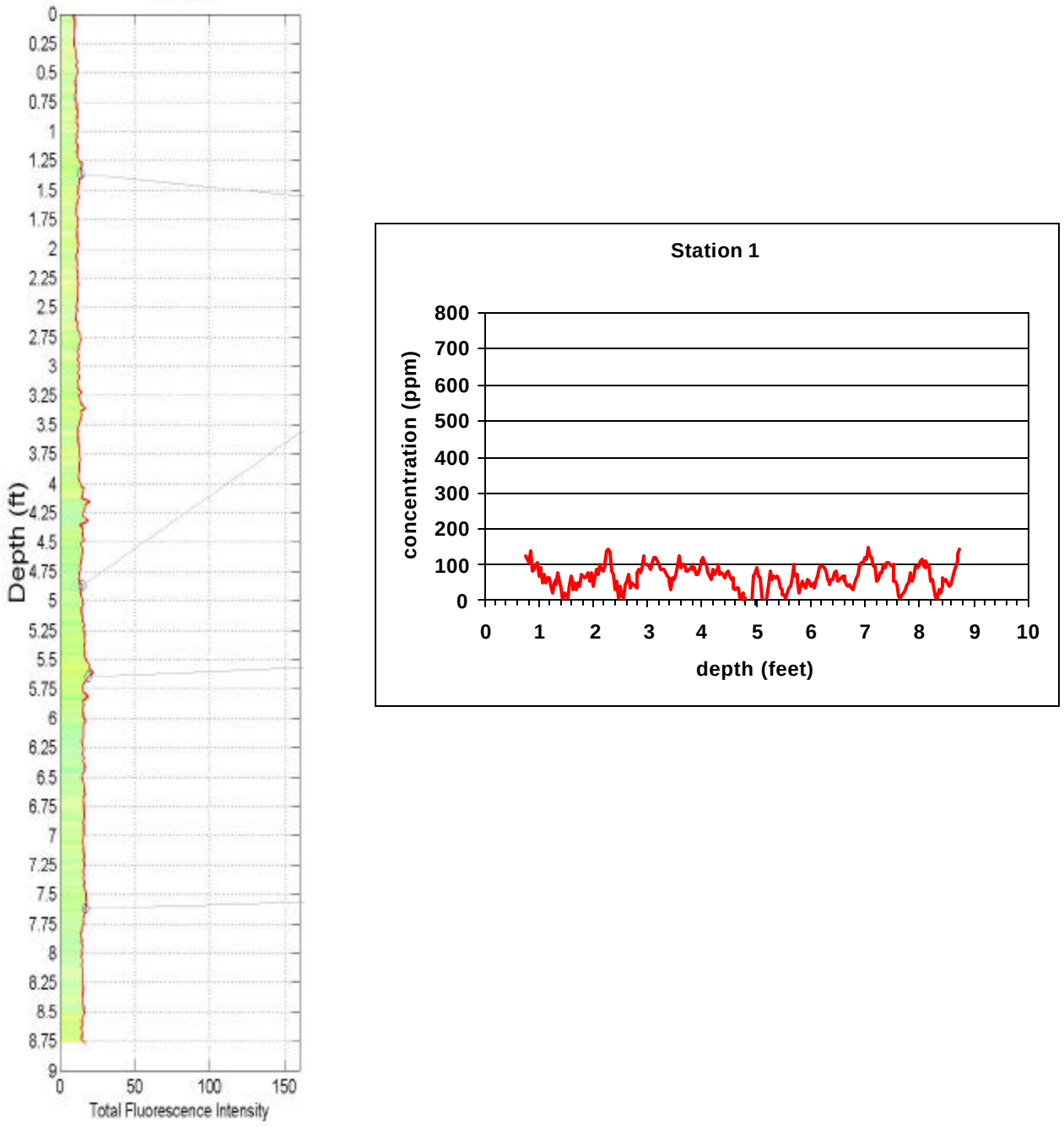

Figure 18. Plots of field fluorescence measurement and chemometric prediction: Station 1. The total fluorescence intensity profile as obtained in the field for station 1 is shown on the left. On the right is the concentration profile of total PAHs obtained after application of chemometric analysis. The concentration profile is a 5-point moving average of individual measurements.

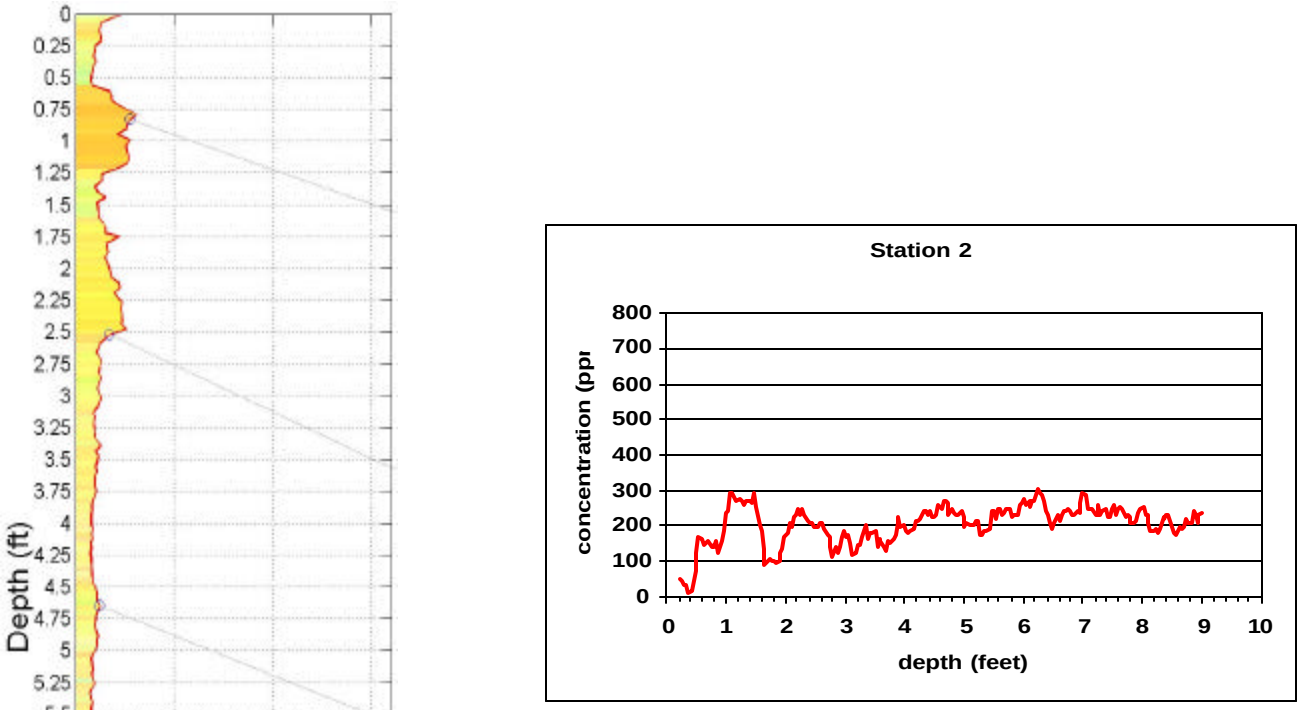

Figure 19. Plots of field fluorescence measurement and chemometric prediction: Station 2. The total fluorescence intensity profile as obtained in the field for station 2 is shown on the left. On the right is the concentration profile of total PAHs obtained after application of chemometric analysis. The concentration profile is a 5-point moving average of individual measurements.

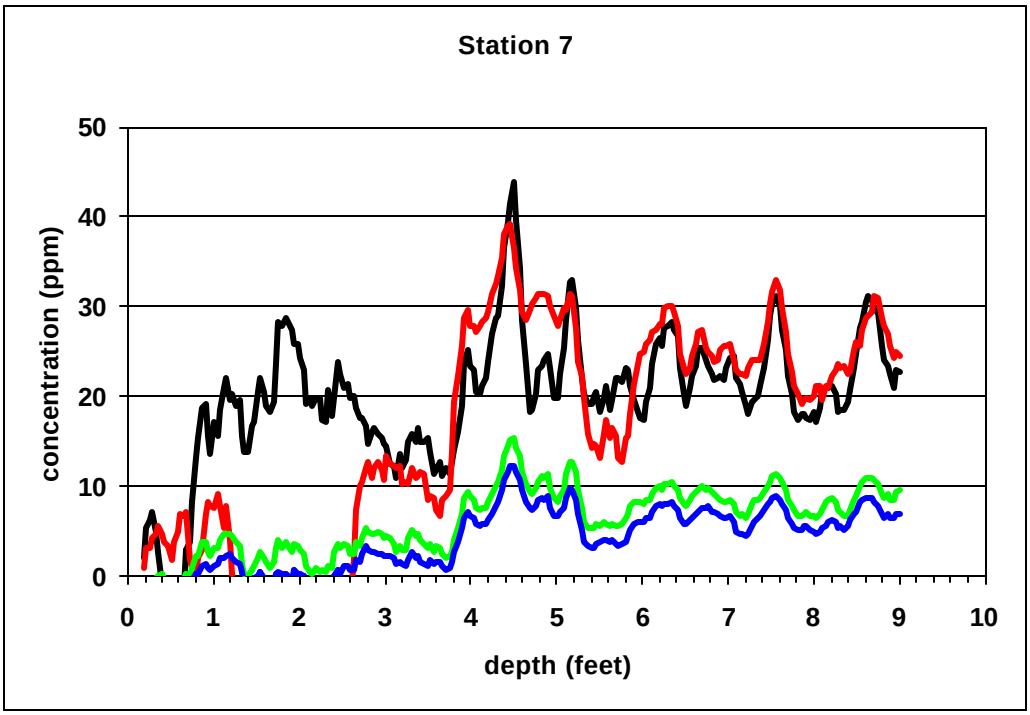

Figure 20. Depth profile of four individual PAH compounds at station 7. Representative multi-ringed aromatic compounds are shown. Blue = fluorene [two aromatic rings]; green = anthracene [three aromatic rings]; red = chrysene [four aromatic rings]; black = benzo(a)pyrene [five aromatic rings]. Trendlines represent the five-point moving average of individual measurements.

A general agreement between total fluorescence intensity and total PAH concentration can be seen in Figures 17 through 19, thereby indicating that a relatively large percentage of total fluorescence is due to the presence of PAH compounds. This generally low background fluorescence is a key feature of these sediments that has allowed for the successful discrimination of PAHs by their fluorescence signals. However, this general agreement does not mean that raw fluorescence intensity data can be used (i.e., without resorting to chemometric analysis). This is exemplified by comparing stations 1 and 2. Total fluorescence intensity below 2.5 feet is low at both stations, with station 2 exhibiting less intensity (typically less than 10%) than station 1 (generally between 10 and 20%). Chemometric data analysis shows the reverse, with considerably higher PAH concentrations in station 2 (200-300 µg/g) than in station 1 (50-100 µg/g). The difference lies in the spectral signature at the two sites. The chemometric analysis uses both spectral and intensity data in the discrimination of PAH from background fluorescence. This can be qualitatively seen by comparing the green color of the total fluorescence plot of station 1 with the predominately yellow color of station 2.

Source Apportionment

The rapidity with which LIF data can be collected, in combination with the ability to identify individual PAH compounds, allows our technique to be used to deduce the sources of contamination in a given stretch of harbor sediment. These source apportionment calculations can be very useful in gaining an overall understanding of general contamination patterns. A detailed investigation into source apportionment was not part of this project, but an example calculation is provided to illustrate the power of this technique.

Previous workers have shown that the relative proportion of certain marker PAHs is indicative of the industrial process that generated the PAHs. Li *et al.* [44] used seven marker compounds to differentiate between three contaminant sources: wood burning, coke oven emissions and highway dust. The primary assumption about the environmental behavior of PAHs that underlies this analysis is that there is no preferential degradation of one PAH over another [44]. Wood burning preferentially produces naphthalene, while coke ovens produce a preponderance of the 5-ring compounds benz(*a*)anthracene and benzo(*a*)pyrene. Highway dust generates a relatively large proportion of pyrene and phenanthrene. These three signatures are shown in Figure 21.

Figure 21 also shows data taken from two sites (station 1 and 7) superimposed on the source signals. A strong highway dust signature is evident in station 7 extending to a depth of at least 8.0 feet. A similar signature is seen in all the other sites upstream of station 5.0 to depths as great as 9.0 feet. These upstream stations are in a portion of the Kinnickinnic River that is not currently dredged (note the depth of water values in Table III). PAH contamination in this stretch of river appears to be primarily caused by runoff of generic highway dust throughout the Milwaukee metropolitan area. The source signatures seen in station 1 are very different. Deep in the core (6.5 feet) the signature has a coke oven component, whereas in the shallower section (1.3 feet) there seems to be a wood-burning component.

Highway dust contamination extending to at least 9.0 feet necessitates a very high sedimentation rate in the upstream portion of the Kinnickinnic River. If it is assumed that large amounts of automobile traffic arose in the Milwaukee area in the mid 1930s, sedimentation rates would be approximately 1.6 inches/year. Although this is surprisingly high, sedimentation rates of between 1.1 and 3.8 inches/year have been reported in the Kinnickinnic River [45]. Furthermore, it is known that during World War II the Kinnickinnic River was dredged for large vessels as far upstream as the Becher Street Bridge and that the sediments have filled in to the current depth of 5.6-8.0 feet since that time.

The enhanced understanding of contaminant sources and sediment dynamics that was gained from source apportionment calculations is evident. This understanding was gained even though the LIF survey was not designed for this purpose and generic literature values were used for source signatures. A thorough attempt at source apportionment would necessitate a multi-variate analysis of the source signatures as well as the sampling of possible source areas and generation of source signals specific to the local area.

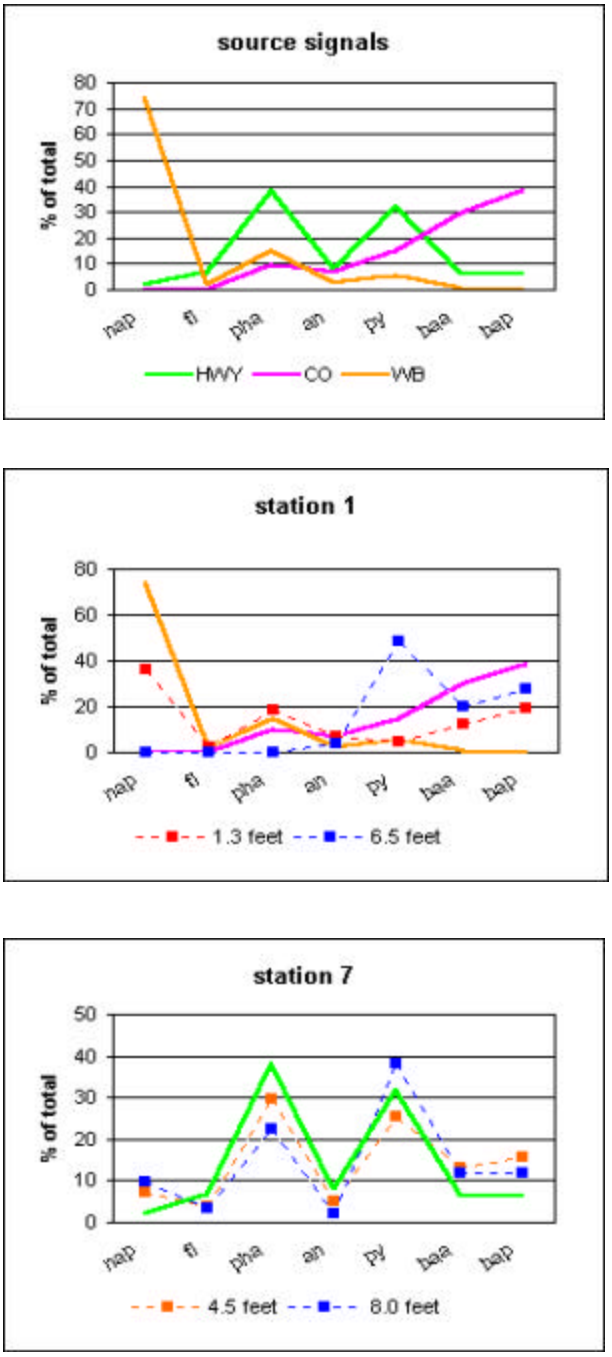

Figure 21. Source apportionment.
Source signals for highway dust (HWY), coke oven emissions (CO) and wood burning (WB) are shown in the top panel. Data from station 7 and station 1 superimposed on source signals are shown in the middle and bottom panels respectively. Source profiles are from [44].

CONCLUSIONS

The results of this study lead directly to the following conclusions:

- The SDV is an effective means for rapidly deploying an LIF probe into submerged harbor sediments. Penetration depths of nine feet can be routinely achieved. Station-to-station turnaround time is ~30 minutes. The SDV has a flexible design that can accommodate any probe that can be fitted to the end of a DPT rod.

- LIF is a viable technique for the *in situ* detection of PAH compounds in harbor sediments. Tracking of total fluorescence alone is not sufficient. A suitable chemometric model must be developed to separate background fluorescence from PAH fluorescence.

- Field testing along the Kinnickinnic River as it enters Milwaukee Harbor shows that LIF can predict individual PAH compounds to within an overall average relative error of 81%. For the 13 PAHs that were found in sufficient quantity to model, the average relative error drops to 28.5% if the sediments that contained less than a minimum threshold limit concentration (between 2 and 10 µg/g) were eliminated. Data repeatability was excellent and the method was shown to apply to sediments that contained a total PAH concentration between 10 and 650 µg/g. The type of sediment for which this technique was tested contained between 1.2% and 5.4% organic carbon and a wide range in sand-silt-clay content.

- The technique provides a rapid, cost-effective, *in situ* means to detect PAH contamination with centimeter-scale vertical resolution. Total fluorescence plots are obtained in real-time, thereby enabling the direction of sampling efforts to be accomplished in the field. The technique is appropriate for screening level assessments of harbor contamination, the direction of dredging efforts, and post-remediation analysis of contaminated sites.

REFERENCES

1 Assessment and Remediation of Contaminated Sediment (ARCS) Program, Final Summary Report. EPA Report EPA-905-S94-001 (1994), 48 pp.

2 Great Lakes Water Quality Board of the International Joint Commission. Position Statement on the Future of Great Lakes Remedial Action Plans (1996), 13 pp.

3 R.C. Knox, D.A. Sabatini, L.W. Cantner. Subsurface Transport and Fate Processes, Lewis Publishers, Boca Raton, FL, 1993.

4 Realizing Remediation, A Summary of Contaminated Sediment Remediation in the Great Lakes Basin, GLNPO Report (1998), 82 pp.

5 A.C. Meigh. Cone Penetration Testing — Methods and Interpretation, Butterworth, London, 1987.

6 D. Lucero. Hazardous Materials Control **1990**, 3, 36.

7 R.V. Overby, M.E. Best. Proceedings of the Air & Waste Management Association **1993**, 15, 133.

8 B.A. Torstensson. Ground Water Monitoring Review **1984**, 4, 131.

9 M. Smolley, J.C. Kappmeyer. Ground Water Monitoring Review **1991**, 11, 101.

10 B. Manchon. Journal of Soil Contamination **1992**, 1, 321.

11 P.D. Kuhlmeier, T.E. Sturdivant. ASTM Special Technical Publication **1992**, 1118, 183.

12 C.Y. Chiang,K.R. Loos, R.A. Klopp. Ground Water **1992**, 30, 428.

13 D.A.Zemo, T.A. Delfino, J.D. Gallinatti, V.A. Baker, L.R. Hilpert. Ground Water Management **1992**, 11, 341.

14 C. Chiang, P. Petkovsky, M. Beltz, S. Rouse, T. Boyd, C. Newell, T. McHugh. Ground Water Management **1993**, 17, 661.

15 B.S. Mines, J.L. Davidson, D. Bloomqvist, T.B. Stauffer. Ground Water Monitoring. Remediation **1993**, 13, 115.

16 D.A. Zemo, Y.G. Pierce, J.D. Gallinatti. Ground Water Monitoring Review **1994**, 14, 176.

17 J.H. Aldstadt, C.H. Batson, A.F. Martin, M.D. Erickson, M.S. Costanza, M.B.J. Foster, T.R. James, P.V. Doskey. Field Analytical Chemistry and Technology **1997**, 1, 239.

18 P.V. Doskey, J.H. Aldstadt, J.M. Kuo, M.S. Costanza. Journal of the Air & Waste Management Association **1996**, 46, 2.

19 K.F. Myers, J.M. Brannon, R.A. Karn, C.B. Price, D.Y. Eng, A.B. Strong, S.S. Cooper. Fourth AWMA/EPA Field Screening Methods for Hazardous Wastes and Toxic Chemicals Symposium, Las Vegas, NV, 1995, p. 177.

20 S.E. Apitz, L.M. Borbridge, G.A. Theriault, S.H. Lieberman. Analysis **1992**, 20, 461.

21 S.E. Apitz, G.A. Theriault, S.H. Lieberman. Proceedings of the International Society of Optical Engineering (SPIE) **1992**, 1637, 241.

22 S.S. Cooper. Device for Measuring Reflectance and Fluorescence of In Situ Soil, U.S. Patent #5,128,882 (1992).

23 S.H. Lieberman, S.E. Apitz, L.M. Borbridge, G.A. Theriault. Proceedings of the International Society of Optical Engineering (SPIE) **1993**, 1716, 393.

24 A. Henderson-Kinney, J.E. Kenny. Spectroscopy **1995**,10, 32.

25 W.C. McGinnis, M. Davey, K.D. Wu, S.H. Lieberman. Proceedings of the International Society of Optical Engineering (SPIE) **1995**, 2367, 2.

26 D.S. Knowles, S.H. Lieberman. Proceedings of the International Society of Optical Engineering (SPIE) **1995**, 2504, 297.

27 J. Lin, S.J. Hart, T.A. Taylor, J.E. Kenny. Proceedings of the International Society of Optical Engineering (SPIE) **1995**, 2367, 70.

28 J. Lin, S.J. Hart, W. Wang, D. Namytchkine, J.E. Kenny. Proceedings of the International Society of Optical Engineering (SPIE) **1995**, 2504, 59.

29 B.J. Nielsen, G. Gillispie, D.A. Bohne, D.R. Lindstrom. Proceedings of the International Society of Optical Engineering (SPIE) **1995**, 2504, 278.

30 W.T. Elam, J.V. Gilfrich. Advances in X-Ray Analysis **1995**, 38, 699.

31 W.T. Elam, J.V. Gilfrich. Proceedings of the International Society of Optical Engineering (SPIE) **1995**, 2367, 59.

32 R. Wisbrun, I. Schechter, R. Niessner, H. Schroder. Proceedings of the International Society of Optical Engineering (SPIE) **1992**, 1716, 2.

33 G.A. Theriault, S.H. Lieberman. Proceedings of the International Society of Optical Engineering (SPIE) **1995**, 2504, 75.

34 J.E. Meisner, W.F. Nicaise, D.C. Stromswold. IEEE Transactions in Nuclear Science **1995**, 42, 288.

35 F.P. Milanovich, S.B. Brown, B.W. Colston. Penetrometer Compatible, Fiber-Optic Sensor for Continuous Monitoring of Chlorinated Hydrocarbons — Field Test Results, UCRL-JC-112182, Lawrence Livermore National Laboratory, Livermore, CA, 1993.

36 E.R. Cespedes,S.S. Cooper, W.M. Davis, W.J. Buttner, W.C. Vickers. Proceedings of the International Society of Optical Engineering (SPIE) **1995**, 2367, 33.

37 ASTM test Method for Deep, Quasi-Static, Cone and Friction Penetration Tests for Soils, ASTM D3441, American Society for Testing and Materials, Philadelphia, PA.

38 S.M. Rudnick, R.F. Chen. Talanta **1998,** 47, 907.

39 R.F. Chen, D.B. Chadwick, S.H. Lieberman. Organic Geochemistry **1997,** 26, 67.

40 H. Marten, T. Naes. Multivariate Calibration, John Wiley and Sons, Chichester, 1996.

41 U.S. Environmental Protection Agency, Office of Solid Waste and Emergency Response, Test Methods for Evaluating Solid Wastes (SW-846), Method 3545A: Pressurized Fluid Extraction, SW-846, Chapter 4.3.1, 2001, Washington, D.C.

42 B. Szostek, J.A. Tinklenberg, J.H. Aldstadt. Chemosphere **1999**, 38, 3131.

43 U.S. Environmental Protection Agency, Office of Solid Waste and Emergency Response, Test Methods for Evaluating Solid Wastes (SW-846), Method 8270C: Determination of Semivolatile Organic Compounds by Capillary GC-MS, SW-846 Chapter 4.3.2, 1997, Washington, D.C.

44 K. Li, E. Christensen, R. Van Camp, I. Imamoglu. Environmental Science & Technology **2001,** 35, 2896.

45 E. Christensen, A. Li, I. Ab Razak, P. Rachdawong, J. Karls. Journal of Great Lakes Research **1997,** 23, 61.